iScience

CellPress
OPEN ACCESS

Article

The Accumulation of Tau-Immunoreactive Hippocampal Granules and Corpora Amylacea Implicates Reactive Glia in Tau Pathogenesis during Aging

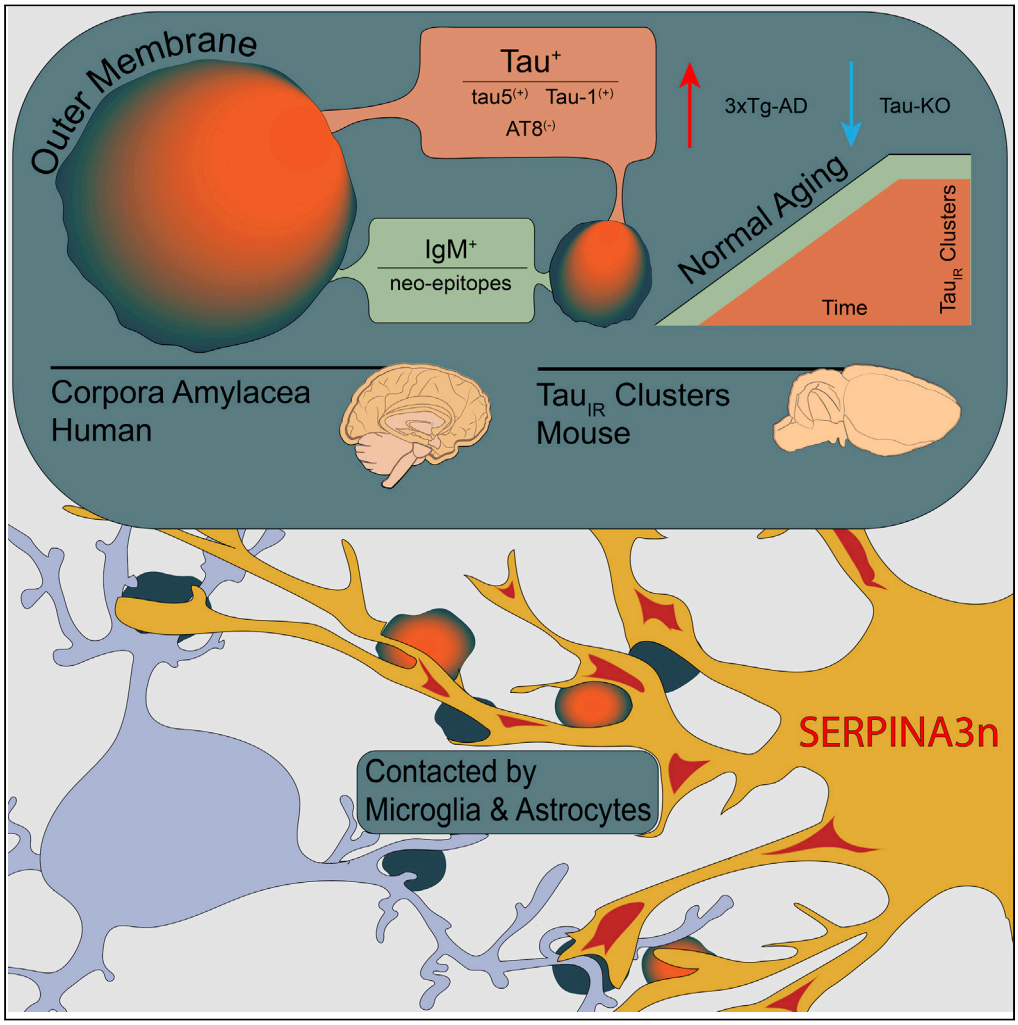

Connor M. Wander, Jui-Heng Tseng, Sheng Song, ..., Rick B. Meeker, David J. Irwin, Todd J. Cohen

toddcohen@neurology.unc.edu

HIGHLIGHTS

Tau is present in mouse hippocampal granules and human corpora amylacea

Tau accumulates with age in hippocampal granules and is accelerated in 3xTg-AD mice

Tau immunoreactive corpora amylacea are present in Alzheimer's disease brain

Age-related tau deposits are associated with reactive astrocytes

Wander et al., iScience *23*, 101255
July 24, 2020
https://doi.org/10.1016/j.isci.2020.101255

iScience

CellPress
OPEN ACCESS

Article

The Accumulation of Tau-Immunoreactive Hippocampal Granules and Corpora Amylacea Implicates Reactive Glia in Tau Pathogenesis during Aging

Connor M. Wander,[1] Jui-Heng Tseng,[2] Sheng Song,[2] Heba A. Al Housseiny,[1] Dalton S. Tart,[1] Aditi Ajit,[2] Yen-Yu Ian Shih,[2] Rebecca Lobrovich,[3] Juan Song,[1,4] Rick B. Meeker,[2] David J. Irwin,[3] and Todd J. Cohen[2,4,5,6,*]

SUMMARY

The microtubule-associated tau protein forms pathological inclusions that accumulate in an age-dependent manner in tauopathies including Alzheimer's disease (AD). Since age is the major risk factor for AD, we examined endogenous tau species that evolve during aging in physiological and diseased conditions. In aged mouse brain, we found tau-immunoreactive clusters embedded within structures that are reminiscent of periodic acid-Schiff (PAS) granules. We showed that PAS granules harbor distinct tau species that are more prominent in 3xTg-AD mice. Epitope profiling revealed hypo-phosphorylated rather than hyper-phosphorylated tau commonly observed in tauopathies. High-resolution imaging and 3D reconstruction suggest a link between tau clusters, reactive astrocytes, and microglia, indicating that early tau accumulation may promote neuroinflammation during aging. Using postmortem human brain, we identified tau as a component of corpora amylacea (CA), age-related structures that are functionally analogous to PAS granules. Overall, our study supports neuroimmune dysfunction as a precipitating event in tau pathogenesis.

INTRODUCTION

One of the defining features of Alzheimer's disease (AD) is the formation of tau species that accumulate with age, initially as soluble tau, then transitioning to tau oligomers and neurofibrillary tangles (NFTs) in end-stage AD brain (Lasagna-Reeves et al., 2012; Maeda et al., 2006). A major challenge when using rodent models of AD is generating robust tau pathology to the extent observed in human tauopathies. Indeed, the formation of tau inclusion pathology in rodents typically requires tau over-expression paradigms, the incorporation of mutant aggregate-prone versions of tau, or prion-like templating to seed tau into an insoluble, hyper-phosphorylated state that resembles that observed in late-stage human tauopathies (Puzzo et al., 2015). Surprisingly, few studies have analyzed normal endogenous tau conformations that emerge during the aging process, well before the onset of cognitive deficits. A better understanding of tau in this early stage could identify pre-pathological tau forms, allow the early detection of tauopathy prior to over symptoms, and potentially even provide a framework for tau-targeted drug discovery.

Recently, we identified a tau species that accumulated in aged wild-type mice (Tseng et al., 2017). This species was distinct from classic tau pathology since it was soluble and immunoreactive with the tau-1 antibody (e.g., tau-1 immunoreactive, or tau-1_{IR}), which detects hypo-phosphorylated tau in the region spanning residues S192–T205 (Binder et al., 1985). The aged tau species accumulated as punctate clusters in the hippocampus and cortex of middle-aged (~12 months old) and older mice (>24 months old) but was nearly undetectable in young mice (<6 months old). Using a cell culture model of acute neuroinflammation, we determined that tau-1_{IR} structures contained tau species that were acetylated (Cohen et al., 2011) and phosphorylated (Drewes et al., 1997) within the microtubule-binding domain (MTBR) (e.g., ac-K280 and p-S262-positive) but not the flanking regions. Thus, we proposed that tau-1_{IR} clusters represent a feature of the aged brain that is accelerated under conditions of neuronal stress or damage. Consistent with this possibility, genetic depletion of the deacetylase HDAC6 in wild-type mice, which confers a neuroprotective effect in some models (Selenica et al., 2014; Zhang et al., 2014a), led to reduced tau-1_{IR} cluster formation. Conversely, neuroinflammatory triggers including lipopolysaccharide (LPS) exposure were associated with

[1]Department of Pharmacology, University of North Carolina, Chapel Hill, NC 27599, USA

[2]Department of Neurology, University of North Carolina, Chapel Hill, NC 27599, USA

[3]Penn Digital Neuropathology Laboratory, Department of Neurology, Perelman School of Medicine, University of Pennsylvania, Philadelphia, PA 19104-4283, USA

[4]UNC Neuroscience Center, University of North Carolina, Chapel Hill, NC 27599, USA

[5]Department of Biochemistry and Biophysics, University of North Carolina, Chapel Hill, NC 27599, USA

[6]Lead Contact

*Correspondence: toddcohen@neurology.unc.edu

https://doi.org/10.1016/j.isci.2020.101255

accumulation of tau-1_{IR} clusters (Tseng et al., 2017). These findings suggested that an age-dependent form of tau might emerge in the brains of vulnerable mice.

Morphologically similar to tau-1_{IR} clusters, carbohydrate-rich deposits known as periodic acid-Schiff (PAS) granules (also referred to as Wirak bodies) are spheroid ~3-μm-diameter structures detected by PAS staining of hippocampal brain sections of aged mice (Cana et al., 2015; Jucker et al., 1994; Kuo et al., 1996; Manich et al., 2014a, 2014b, 2015, 2016; Wirak et al., 1991). In addition, similarly spherical, age-related structures known as corpora amylacea (CA) have been described in human brain (Auge et al., 2017, 2018, 2019; Manich et al., 2016; Singhrao et al., 1993). Both PAS granules and CA are thought to emerge during aging as a result of abnormal or pathological processes, potentially arising from diverse stressors including oxidative stress (Porquet et al., 2013), neuroinflammation (Tseng et al., 2017), or environmental triggers such as fungal (Pisa et al., 2016) or viral (Libard et al., 2014) infection. Like tau-1_{IR} clusters, PAS granules increase in the aged mouse brain (Manich et al., 2014a). Primarily thought to be composed of glycoproteins and carbohydrate moieties, the protein constituents of PAS granules remain poorly characterized, largely due to false-positive PAS granule detection from non-specific IgM components present in many natural and commercially available antibodies (Manich et al., 2015). In light of this confounding issue, the mechanism of PAS granule biogenesis and its role in neurodegenerative disease has been a highly debated topic.

At the ultrastructural level, PAS granules were shown to contain degenerating cytoplasmic organelles including mitochondria, irregular vacuolar structures, fragmented cytoskeletal components, and breakdown products derived from degenerating neurons and astrocytes (Kuo et al., 1996; Manich et al., 2014a; Mitsuno et al., 1999). A link between tau, PAS granules, and AD is bolstered by the presence of degenerating dendrites immediately surrounding PAS deposits (Manich et al., 2014a), as well as the potential identification of tau and other MAPs within CA by proteomics approaches (Pisa et al., 2018). Furthermore, a significant correlation was observed between PAS granule formation and hippocampal-dependent spatial memory defects (Jucker et al., 1994; Knuesel et al., 2009). Recent findings indicate that CA or PAS granules may be engulfed by macrophages after they are extruded from the brain into the cerebrospinal fluid (CSF) (Riba et al., 2019). Thus, PAS granules may act in a protective capacity during aging to isolate or limit the accumulation of damaged, misfolded, and aggregated proteins including tau. Excessive PAS granule formation, coupled with its failed clearance, could exacerbate disease pathology and promote neurodegeneration. Connecting these structures to the progression of AD and other tauopathies remains an unresolved issue that has major implications for brain aging, AD pathology, and cognitive decline.

Here, we performed a detailed characterization of tau-1_{IR} structures and found striking parallels between tau-1_{IR} clusters and mouse PAS granules. We then validated the specific immunoreactivity of tau-1 and tau5 mouse monoclonal antibodies using genetic tau-knockout mice and immunoadsorption techniques. We show that the formation of tau-immunoreactive clusters, which accumulate predominantly in the CA1 region, are accelerated in the 3xTg-AD model mice and are present in the hippocampus of aged and AD postmortem human brain. High-resolution 3D microscopy indicates that the cluster-associated pool of tau is engaged by astrocytic and microglial processes. Overall, our data highlight mouse PAS granules and human CA as unanticipated hubs for the emergence of tau species that may be linked to the evolution of tau pathology in normal aging, AD, and related tauopathies.

RESULTS

Characterizing Tau-1_{IR} Cluster Formation by Tau Epitope Immunoreactivity

In our previous study, we showed that the non-phosphorylation-specific monoclonal tau-1 antibody and the tau-oligomer-specific polyclonal T22 antibody both partly labeled hippocampal age-related clusters in wild-type mice (Tseng et al., 2017) (Table S1). To evaluate tau-1_{IR} clusters under pathological conditions, we performed double-labeling immunofluorescence on wild-type and transgenic AD mice (3xTg-AD). These mice harbor three mutations associated with familial AD (APP Swedish, MAPT P301L, and PSEN1 M146V), which drive cortical Aβ plaque deposition at 3–4 months of age, whereas transgenic human tau pathology is not observed robustly until around 12 months of age, at which point cognitive deficits become more apparent (Oddo et al., 2003). Tau-1_{IR}/$T22_{IR}$ clusters were detected in the molecular layer (ML), stratum oriens (SO), and prominently in the stratum radiatum (SR) of aged 3xTg-AD mice (Figure 1A). These observations are consistent with the prior detection of PAS granules in the SR and nearby hippocampal regions such as the stratum lacunosum moleculare (SLM) (Manich et al., 2014b), indicating that tau-1_{IR} clusters and

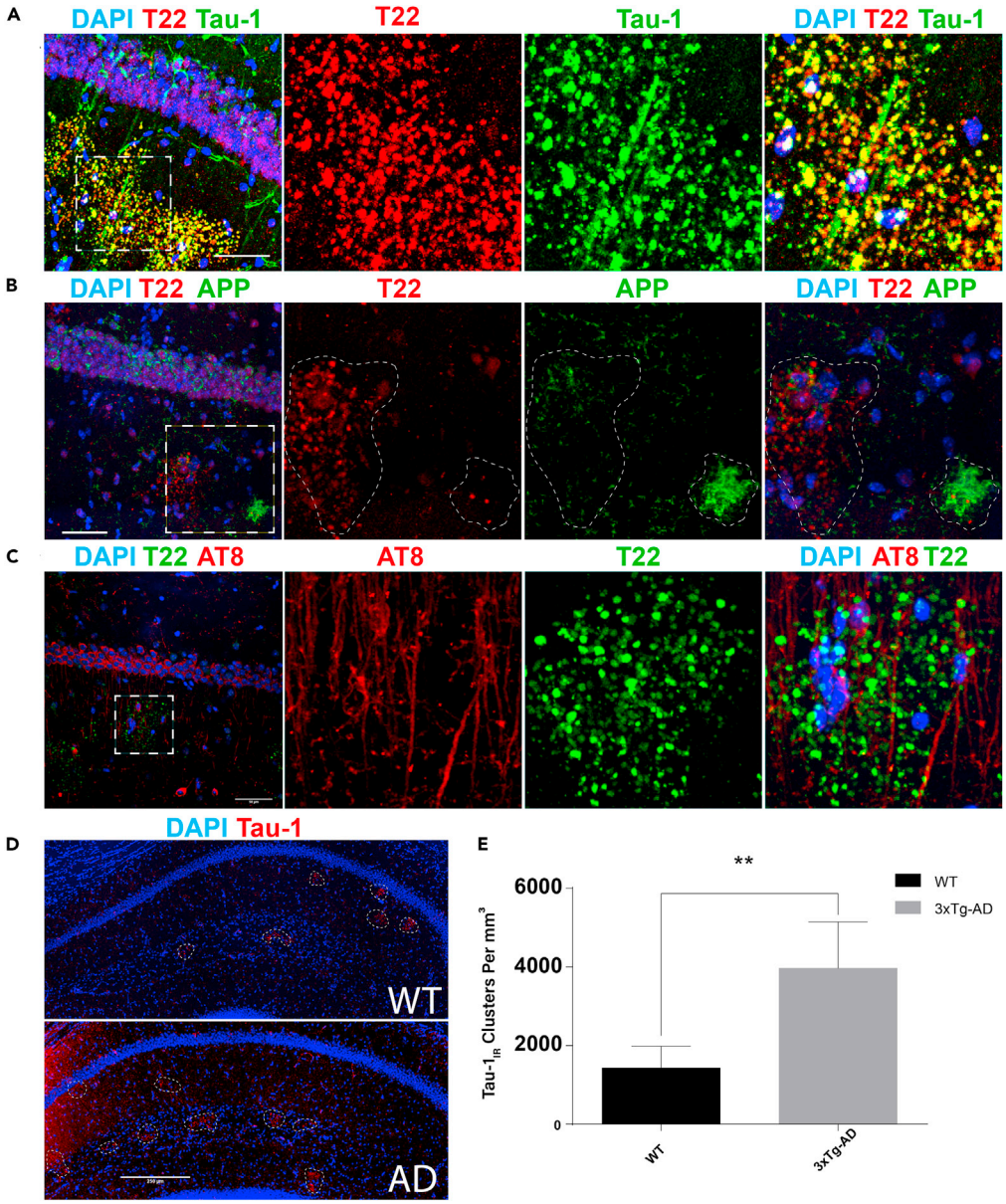

Figure 1. Tau-Immunoreactive Clusters in the Hippocampus Are Distinct from Plaque Pathology in 3xTg-AD Mice

(A) Immunofluorescent confocal images of aged (21-month-old [mo]) 3xTg-AD mice indicate that Tau-1 (green) and T22 (red) co-localize in granules in the CA1 and SR.

(B) T22 (red) does not co-localize with plaques (6E10) or neuronal soma (green) within the CA1 and SR.

(C) AT8-immunoreactive neuronal soma and axons (red) associate, but do not co-localize, with T22-positive granules (green) in the CA1 or SR.

(D) Representative immunofluorescent images of 3xTg-AD and WT hippocampal fields captured by confocal microscopy at 40x magnification. Dashed circles indicate tau-1_{IR} clusters (red).

(E) Quantification of tau-1_{IR} clusters showing that they are significantly elevated in the hippocampi of 6-mo 3xTg-AD mice when compared with controls.

Scale bars, 50 μm (A–C), 250 μm (D). Statistical significance was assessed using Student's t test from N = 4 biological replicates (**$p < 0.01$). Error bars represent SEM. See also Figure S1.

PAS granules correspond, at least morphologically, to identical age-related deposits. Importantly, analysis of Aβ plaques in 3xTg-AD mice, detected with the 6E10 monoclonal antibody, showed that tau-1_{IR} clusters were not associated with plaque pathology in these regions (Figure 1B).

To determine whether tau-1_{IR} clusters in wild-type (WT) and 3xTg-AD mice contain phosphorylated tau, we evaluated their immunoreactivity with AT8, a monoclonal antibody commonly used to mark NFT pathology, which detects tau phosphorylated at S202/T205. Consistent with tau-1 and AT8 targeting complimentary epitopes (Szendrei et al., 1993), we found that tau-1_{IR}/$T22_{IR}$ clusters were AT8-negative in the SR of 3xTg-AD mice (Figure 1C), indicating enrichment for hypo-phosphorylated tau, at least within the region detected by tau-1 (residues S195-T205) and T22 (oligomeric) antibodies. Quantification of tau-1_{IR} cluster density from hippocampal sections of 6-month-old mice showed a significant increase from 1,425 granules/mm^3 in WT to 3,965 granules/mm^3 in 3xTg-AD mice (Figures 1D and 1E). The difference between genotypes gradually normalized as the mice aged (Figure S1A). These results suggest that tau-1_{IR} cluster formation is accelerated at early stages in an AD mouse model and support the independent spatial accumulation of tau clusters and Aβ in the aging hippocampus.

Evaluating Tau as a Component of PAS Granules

To confirm the incorporation of tau into PAS granules, we performed genetic validation experiments using tau knockout (TKO) mice to evaluate the specificity of tau within PAS granules. Surprisingly, although total tau (K9JA) immunoreactivity was absent, quantification of confocal images revealed that tau-1_{IR} clusters were detectable yet significantly less dense in the hippocampi of 23-month-old TKO mice (~9,000 granules/mm^3) compared with age-matched WT mice (~14,400 granules/mm^3) (Figures 2A–2C), indicating that tau depletion reduced but did not eliminate tau-1 immunoreactivity. Immunoblotting of hippocampal lysates showed the expected tau depletion (Figure 2D), excluding the potential for any residual tau expression in the TKO mice.

To further address the presence of tau clusters in TKO mice, we investigated their molecular and histological properties. Tau-1_{IR} clusters are highly reminiscent of PAS granules, also known as Wirak bodies, which form in aged mouse brain (Wirak et al., 1991). Mass spectrometry-based proteomics of related CA deposits from human brain hinted that tau and related MAPs may be present within these structures (Pisa et al., 2018), but this has not been confirmed or thoroughly investigated. Intriguingly, PAS granules and CA comprise neo-epitopes containing carbohydrates that are recognized by natural and commercially available antibodies containing a non-specific IgM fraction (Manich et al., 2015). Therefore, to clarify whether the tau-1_{IR} clusters contain tau or rather result from non-specific immunohistochemical detection due to anti-IgM immunoreactivity, we performed a series of experiments using more highly specific immunohistological approaches. We used isotype-specific anti-mouse IgG and anti-mouse IgM secondary antibodies to distinguish among the components found within the primary tau antibodies (Table S1).

Tau-1_{IR} and $tau5_{IR}$ clusters were indeed detected with anti-mouse IgM-specific secondary antibodies in aged mice (Figures 3A and 3B, green) but not in young 2-month-old WT or AD mice (Figure S1B), suggesting a non-specific IgM component is present in these monoclonal antibodies. This result is not unexpected, as many commercial antibodies contain trace amounts of IgM antibodies directed against poorly defined neo-epitopes that can lead to false-positive detection of PAS granules or analogous structures (Auge et al., 2018). We therefore subclassified tau_{IR} clusters into anti-mouse IgG-specific and anti-mouse IgM-specific (anti-IgM, μ-chain specific) granules using secondary antibodies against tau-1 (anti-IgG2a, γ-chain specific) or tau5 (anti-IgG1, γ-chain specific) (Table S2). Although the tau-1 and tau5 monoclonal antibodies harbor an IgM component, we observed anti-mouse IgG-specific tau_{IR} granules within the anti-mouse IgM-specific granules, indicating that a pool of tau does indeed localize to PAS granules in 3xTg-AD mice (Figures 3A and 3B, red). Moreover, we excluded any non-specific IgG immunoreactivity using an isotype control antibody (Figure S2). Further confirming the presence of tau within these structures, tau_{IR} granules were not detectable using anti-mouse IgG-specific secondary antibodies in TKO mice that lack the tau protein, despite the fact that anti-mouse IgM-specific immunoreactivity remained (Figures 3A and 3B, see TKO panel).

As an IgM and IgG1-containing positive control primary antibody, we used a monoclonal anti-Reelin antibody (clone G10) and confirmed the expected non-specific IgM component that was previously shown to label PAS granules, referred to as "Reelin plaques" (Doehner et al., 2010; Knuesel et al., 2009; Manich et al., 2016). Both anti-mouse IgG1-specific and anti-mouse IgM-specific secondary antibodies labeled Reelin granules in the 3xTg-AD mouse, and neither signal was effectively depleted in TKO mice (Figure 3C).

To further validate the specificity of tau-1 and tau5 antibodies, we performed immunoadsorption experiments to block the monoclonal antibody epitopes and hence neutralize tau immunoreactivity prior to

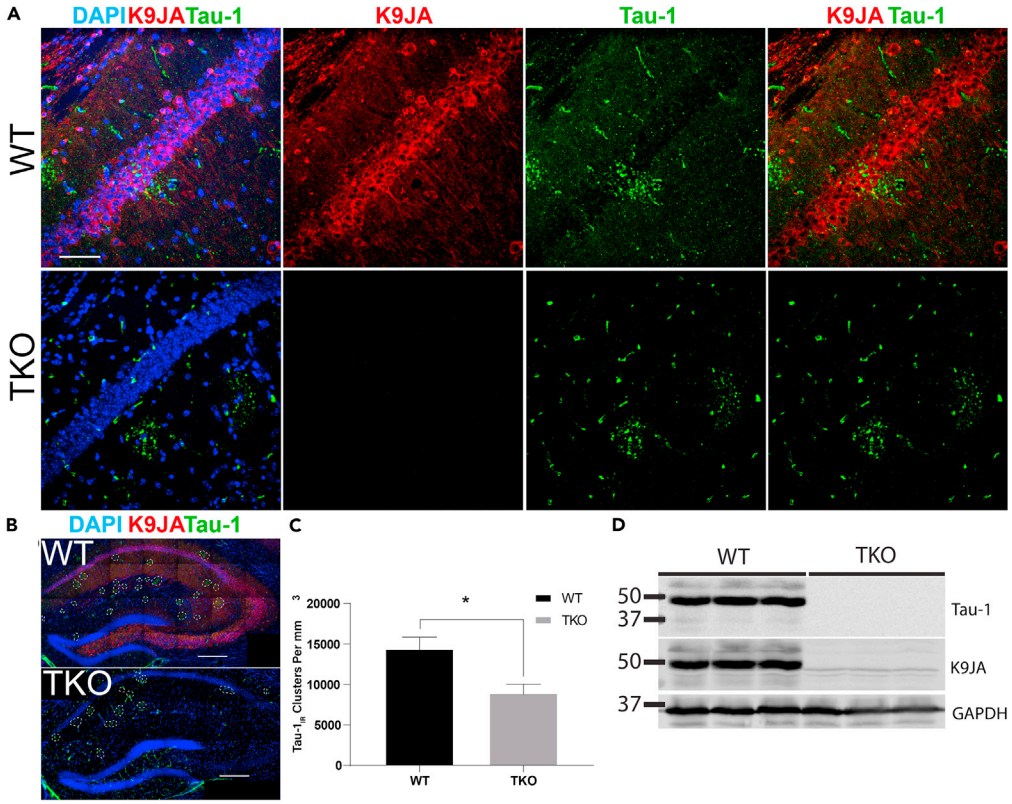

Figure 2. Tau-Immunoreactive Clusters Are Reduced, but Not Eliminated, in Tau KO Mice When Detected with Pan-Reactive Secondary Antibodies

(A) Immunofluorescent confocal images of aged (23-mo) wild-type (WT) and tau knockout (TKO) mice show immunoreactivity with K9JA (red) and tau-1 (green) in the CA1 and SR of WT mice, with only tau-1_{IR} cluster immunoreactivity in TKO mice.

(B) Representative images of full hippocampal fields in aged WT and TKO mice captured by confocal microscopy at 40x magnification.

(C) Quantification of tau-1_{IR} cluster density showing a reduction in granules in 23-mo TKO mice when compared with age-matched WT mice.

(D) Immunoblots of tau (tau-1, K9JA) and GAPDH in 23-mo WT and TKO mouse hippocampal lysates confirm the absence of tau expression in TKO mice.

Scale bars, 50 μm (A), 250 μm (B). Statistical significance was assessed using a Student's t test from N = 4 biological replicates (*$p < 0.05$). Error bars represent SEM. See also Figure S2.

immunofluorescence analysis. To deplete the tau signal with native tau isoforms, we used either recombinant human tau protein (2N4R full-length tau) or a brain-derived MAP-rich fraction (containing tau) isolated by temperature-induced tubulin polymerization, ionic exchange chromatography, and high salt elution. The MAP mixture contains multiple neuronal tau and MAP isoforms that we confirmed by immunoblotting of serially diluted MAP-rich fractions (Figure 4A). Pre-incubating the tau5 or tau-1 antibodies with the MAP-rich fraction or with recombinant full-length tau led to antibody neutralization and a reduction in the anti-mouse IgG-specific detection of tau in dendrites and granules of 3xTg-AD mice (Figures 4B and 4C) as well as aged WT mice (Figures S3A and S3B). Pre-incubation of the tau-1 primary antibody with a purified peptide containing only the tau-1 epitope sequence nearly eliminated the anti-mouse IgG-specific detection of tau-1_{IR} granules (Figure 4D), whereas anti-mouse IgM-specific granules remained. Therefore, combining genetic and histological validation controls, we conclude that tau is a *bona fide* constituent of PAS granules that accumulates in the aged mouse brain.

We also investigated the possibility of MAP2 accumulation within tau_{IR} clusters. Multiple MAPs were found by mass spectrometry analysis of CA isolated from human brain tissue, with MAP2 being the most commonly observed peptide (Pisa et al., 2018). We used a mouse monoclonal MAP2 antibody (IgG1)

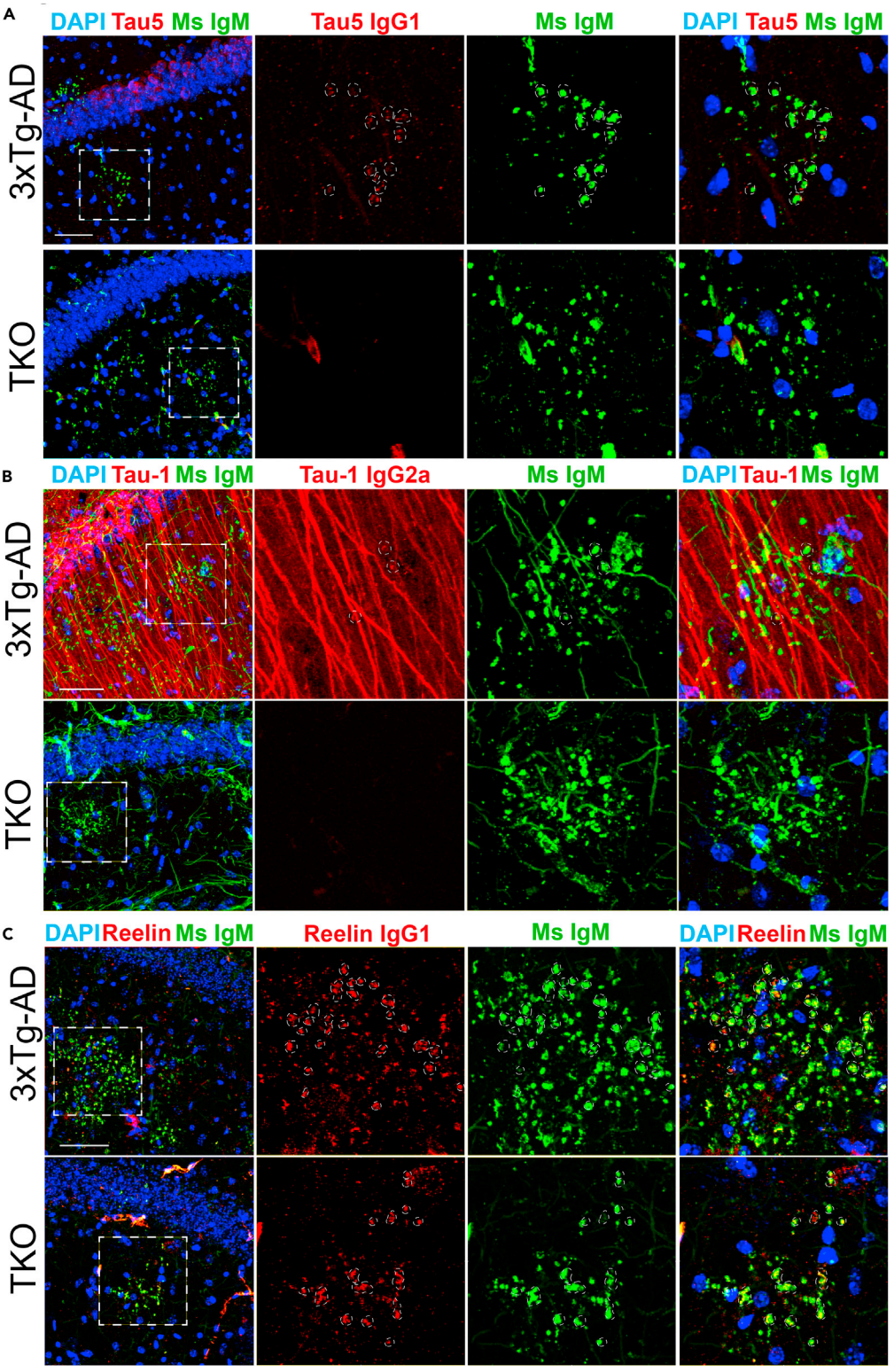

Figure 3. Analysis of Hippocampal Tau Clusters Using Isotype-Specific Immunodetection

(A) Immunofluorescent confocal images of aged (23-mo) 3xTg-AD and TKO mice using isotype-specific secondary antibodies. Tau5 detects tau granules when labeled with an anti-mouse IgM μ-chain-specific secondary antibody (Ms IgM,

Figure 3. *Continued*
green) in both genotypes and partially detects tau granules when labeled with an anti-mouse IgG1 γ-chain-specific secondary antibody (Tau5 IgG1, red) in 3xTg-AD but not TKO mice.
(B) Tau-1 detects tau granules when labeled with an anti-mouse IgM μ-chain-specific secondary antibody (Ms IgM, green) in both genotypes and partially detects tau granules when labeled with an anti-mouse IgG2a γ-chain-specific secondary antibody (Tau-1 IgG2a, red) in 3xTg-AD mice but not TKO mice.
(C) Reelin partially detects granules when labeled with both anti-mouse IgM μ-chain-specific (Ms IgM, green) and anti-mouse IgG1 γ-chain-specific (Reelin IgG1, red) secondary antibodies in both 3xTg-AD and TKO mice.
Scale bars, 50 μm; dashed white circles indicate regions of co-localization. See also Figure S3.

that contains an IgM component in conjunction with isotype-specific secondary antibodies and observed that MAP2 labeled with anti-mouse IgG1-specific secondary antibodies reliably marked dendrites but was not immunoreactive within anti-mouse IgM-specific clusters in aged mice (Figure S4). We did, however, observe PAS granules closely associated with MAP2-positive dendrites, suggesting that PAS granules may partly originate from neurons.

Tau-1_{IR} Cluster Formation Is Associated with Reactive Astrocytes

Previous studies support a glial origin of PAS granules, as > 60% of these structures are reported to associate with glial fibrillary acidic protein (GFAP)-immunoreactive astrocytic processes (Akiyama et al., 1986; Jucker et al., 1994; Kuo et al., 1996; Madhusudan et al., 2009; Manich et al., 2014a; Nakamura et al., 1995; Robertson et al., 1998). Moreover, we showed that tau-1_{IR} clusters correlate with inflammatory microglia in the hippocampus (Tseng et al., 2017). We therefore explored the interactions of anti-mouse IgG-specific tau_{IR} granules with microglia and astrocytes. Iba-1-positive microglial processes were in close proximity with anti-mouse IgG-specific tau_{IR} granules and were observed surrounding these structures (see arrowheads marking these interactions) (Figure 5A). More prominently, GFAP-positive astrocytic processes were strongly co-localized with anti-mouse IgG-specific tau_{IR} granules, and the astrocytic somas were frequently at the center of individual tau_{IR} cluster patches (Figure 5B). Isotype-specific staining using a mouse monoclonal GFAP antibody detected a substantial IgM component, whereas the IgG component of the GFAP antibody labeled with anti-mouse IgG1-specific secondary showed very close juxtaposition of astrocytic processes that terminated with PAS granules (Figure S5).

Both astrocytes and microglia are known to alter synapses, and synaptic dysfunction is observed under neuroinflammatory conditions including LPS exposure, which increases PAS granule burden and astrocyte reactivity throughout aging (Chen et al., 2014). Reactive astrocytes may therefore represent a major source of neuronal toxicity via the release of factors that induce microglial activation throughout normal aging and in many neurodegenerative disorders (Liddelow et al., 2017). Astrocytic reactivity is known to increase owing to inflammation and injury, and astrocytes increasingly display transcript profiles indicative of a neurotoxic A1 phenotype that arises during normal aging in rodents (Clarke et al., 2018). Among the most prominent up-regulated genes throughout aging was Serpina3n, a serine-threonine protease inhibitor (Baker et al., 2007), the expression of which increases sharply during normal aging in the rodent hippocampus, but not the cortex, mirroring the pattern of PAS granule formation (Vanni et al., 2017). Given their close proximity, we hypothesized that the formation of PAS granules during aging could coincide with an increase in astrocyte reactivity.

To investigate this possibility, we used *in situ* RNA probes and performed double labeling using a combination of RNA probes and antibodies marking astrocytes (GFAP) and PAS granules (T22) in aged mouse brain. As expected, the negative control RNA probe (DapB) showed limited reactivity (Figure 5C, bottom row), whereas abundant signal was detected with the positive control probe (Mm-PpiB) (Figure 5C, middle row), a factor involved in collagen formation. Using the Serpina3n probe (Mm-Serpina3n), we found that Serpina3n expression was enriched in the soma and processes of the same astrocytes that also harbored tau_{IR} clusters (Figure 5C, top row, see co-localized regions marked by arrowheads). These results suggest that tau granule formation is linked to increased astrocytic reactivity during normal rodent aging.

To further visualize the association of microglia and astrocytes interacting with tau granules, we used 3D reconstruction imaging techniques (Figure 6). The analysis revealed extensive interactions between anti-IgG-specific $tau5_{IR}$ granules and either microglia (Figure 6A) or astrocytes (Figure 6B) (see arrowheads marking regions of co-localization). The prominent association of astrocytes, in particular, with PAS granules was even more apparent with GFAP labeling and high-resolution 3D reconstruction of the astrocytic processes wrapping around PAS granules (labeled with anti-IgM-specific secondary antibodies to label

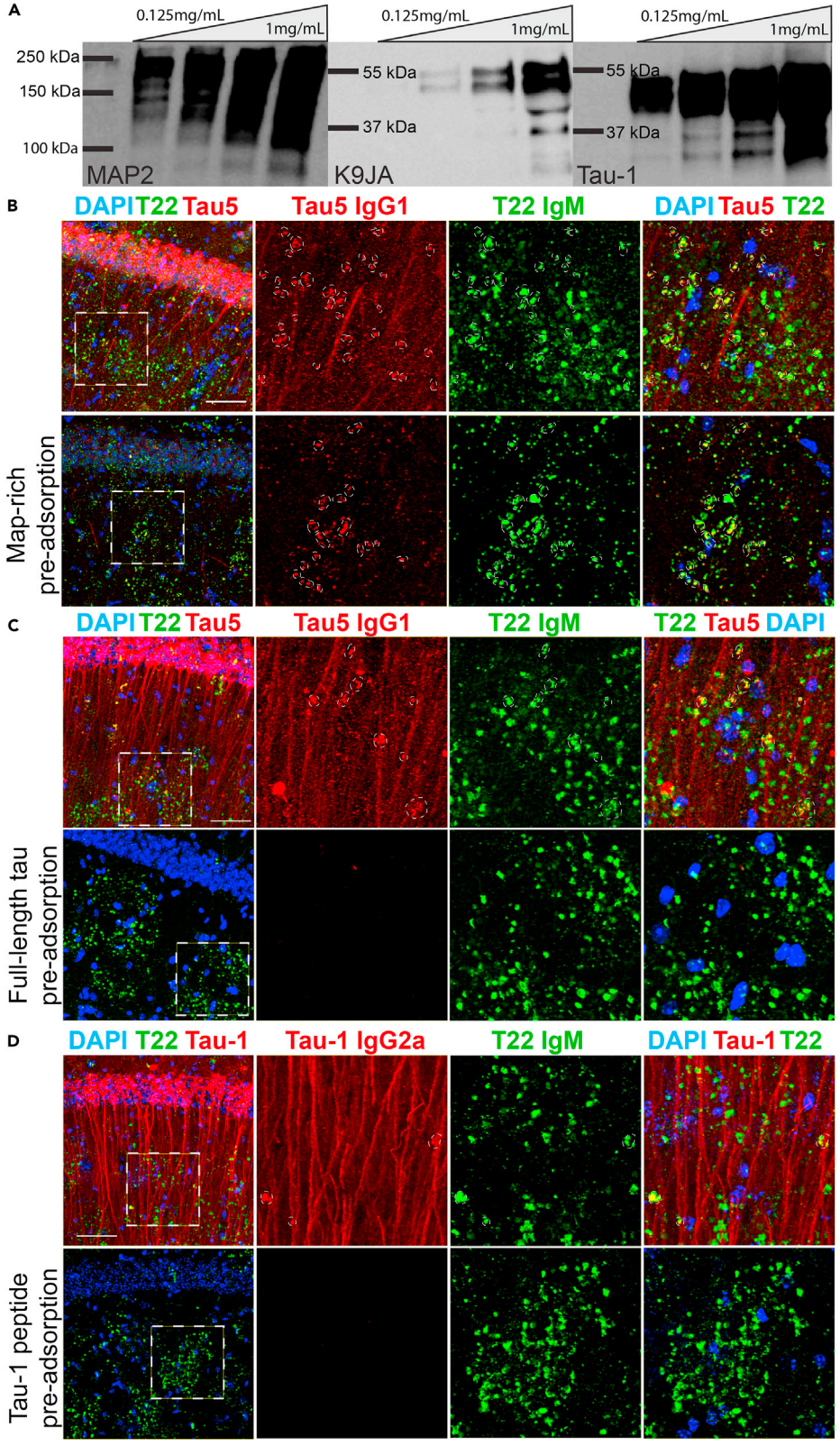
A
0.125mg/mL
1mg/mL
250 kDa
150 kDa
100 kDa
MAP2
55 kDa
37 kDa
K9JA
Tau-1
B
DAPI T22 Tau5
Tau5 IgG1
T22 IgM
DAPI Tau5 T22
Map-rich pre-adsorption
C
DAPI T22 Tau5
Tau5 IgG1
T22 IgM
T22 Tau5 DAPI
Full-length tau pre-adsorption
D
DAPI T22 Tau-1
Tau-1 IgG2a
T22 IgM
DAPI Tau-1 T22
Tau-1 peptide pre-adsorption

Figure 4. Analysis of Tau Clusters Following Epitope Neutralization by Immunoadsorption

(A) Immunoblots of MAP-rich fractions (MRFs) from porcine brain that were used to pre-adsorb tau-1, tau5, and MAP2 primary antibodies showing MAP2 and tau (K9JA, tau-1) immunoreactivity.

(B) The tau5 antibody detects granules when labeled with an anti-mouse IgM μ-chain-specific secondary antibody (Ms IgM, green), labels both dendrites and granules when labeled with an anti-mouse IgG1-specific secondary antibody (Tau5 IgG1, red), and is partially pre-adsorbed when neutralized with MRF, whereas anti-mouse IgM-specific granules (Ms IgM, green) remain in 21-mo 3xTg-AD mice.

(C) Tau5 anti-mouse IgG1-specific (Tau5 IgG1, red) immunoreactivity is neutralized with recombinant full-length (2N4R isoform) tau protein, whereas anti-mouse IgM-specific granules (green) remain in 21-mo 3xTg-AD mice.

(D) The tau-1 antibody detects granules when labeled with anti-mouse IgM μ-chain-specific secondary antibody (Ms IgM, green), detects dendrites and some, but not all, granules when labeled with anti-IgG2a secondary antibody (Tau-1 IgG2a, red) in 21-mo 3xTg-AD mice. Tau-1 anti-mouse IgG2a-specific immunoreactivity is neutralized by the purified tau-1 peptide, whereas anti-mouse IgM-specific (Ms IgM, green) immunoreactivity remains. Scale bars, 50 μm, dashed white circles indicate regions of co-localization.

See also Figure S4.

the entire PAS granule pool) (Figure 6C). Our findings strongly support the notion that microglia and reactive astrocytes are intimately associated with anti-mouse IgG-specific tau_{IR} granules.

Next, we sought to corroborate our observations in mice with human postmortem brain tissue. Corpora amylacea (CA) in humans are thought to represent structural and functional homologues of mouse hippocampal PAS granules (Auge et al., 2019). Therefore, we analyzed hippocampal tissue sections from human control subjects and patients with AD with polyclonal GFAP and monoclonal tau5 antibodies, followed by labeling with isotype-specific secondary antibodies (Figures 7A–7C). We closely monitored anti-mouse IgG-specific tau5 immunoreactivity within CA structures, which are routinely observed in the subpial regions of the hippocampus. Consistent with our findings in mice, tau-positive CA were marked with both anti-mouse IgM-specific and anti-mouse IgG-specific secondary antibodies and were often in close proximity to GFAP-positive astrocytes (Figures 7A and S6, arrowheads indicate CA). Immunoadsorption of the tau5 primary antibody with full-length recombinant tau protein eliminated anti-mouse IgG-specific tau5 immunoreactivity in human CA, whereas anti-mouse IgM-specific immunoreactivity remained (Figures S7A and S7B). In many instances, we observed striking hollowed-out or dome-like CAs that were prominently tau5 immunoreactive using anti-mouse IgG-specific secondaries in AD brain (Figure 7B), which was further analyzed by (1) average-Z projection and orthogonal views (Figure 7C-i), (2) single confocal planes (Figure 7C-ii), and (3) 3D reconstruction analysis using IMARIS software (Figures 7D-i and 7D-ii, alternate views). The hollowed appearance of tau-positive CA could potentially arise from the harsh antigen retrieval process that may remove the internal CA contents but leave membrane-associated tau intact. In AD brain, we observed typical neuritic tau pathology that was largely enveloped by GFAP-positive processes and was in close proximity to CA membrane-associated tau (Figure S6).

We complemented the human confocal imaging with immunohistochemical (IHC) analysis of a panel of cases using isotype-specific horseradish peroxidase (HRP)-conjugated secondary antibodies to label tau-positive CA (anti-mouse IgG2a or anti-mouse IgG1). Our data confirm that total tau, as detected with anti-mouse IgG-specific secondary antibodies, labels human CA, whereas hyper-phosphorylated tau, detected with AT8 is largely excluded (Figure 7E). However, in some instances, we observed AT8 and tau5 immunoreactivity surrounding and encircling CA (Figure 7F). Based on tau immunoreactivity within CA using AT8, tau5, and tau-1 antibodies, we scored tau-positive CA intensity using a semi-quantitative grading scheme from 0 to 3 in increments of 0.5 (Table S3). We observed a negative correlation for both tau5 ($p = 0.0325$) and tau-1 ($p = 0.0285$) immunoreactive CA as a function of increasing Braak stage (Figures S7C and S7D), suggesting tau-immunoreactive CA decrease with increasing burden of insoluble tau pathology in AD. We note that, although this is significant, given the variance in the data, additional studies with larger cohorts are warranted to further correlate tau immunoreactive CA with neuropathological, genetic, and/or cognitive measures of disease progression.

To the best of our knowledge, CA-enriched tau species have not been previously characterized in human brain. Thus, we refer to this tau species as CA-associated tau, or CA-tau. Our IHC analysis indicates that CA-tau is often tau-1 and tau5 immunoreactive within the CA core, whereas phosphorylated tau (AT8-positive), when present, is largely restricted to the CA membrane. Overall, our study highlights mouse PAS granules and human CA as novel hubs involved in tau processing and potential determinants of tau pathogenesis during the aging process and in AD.

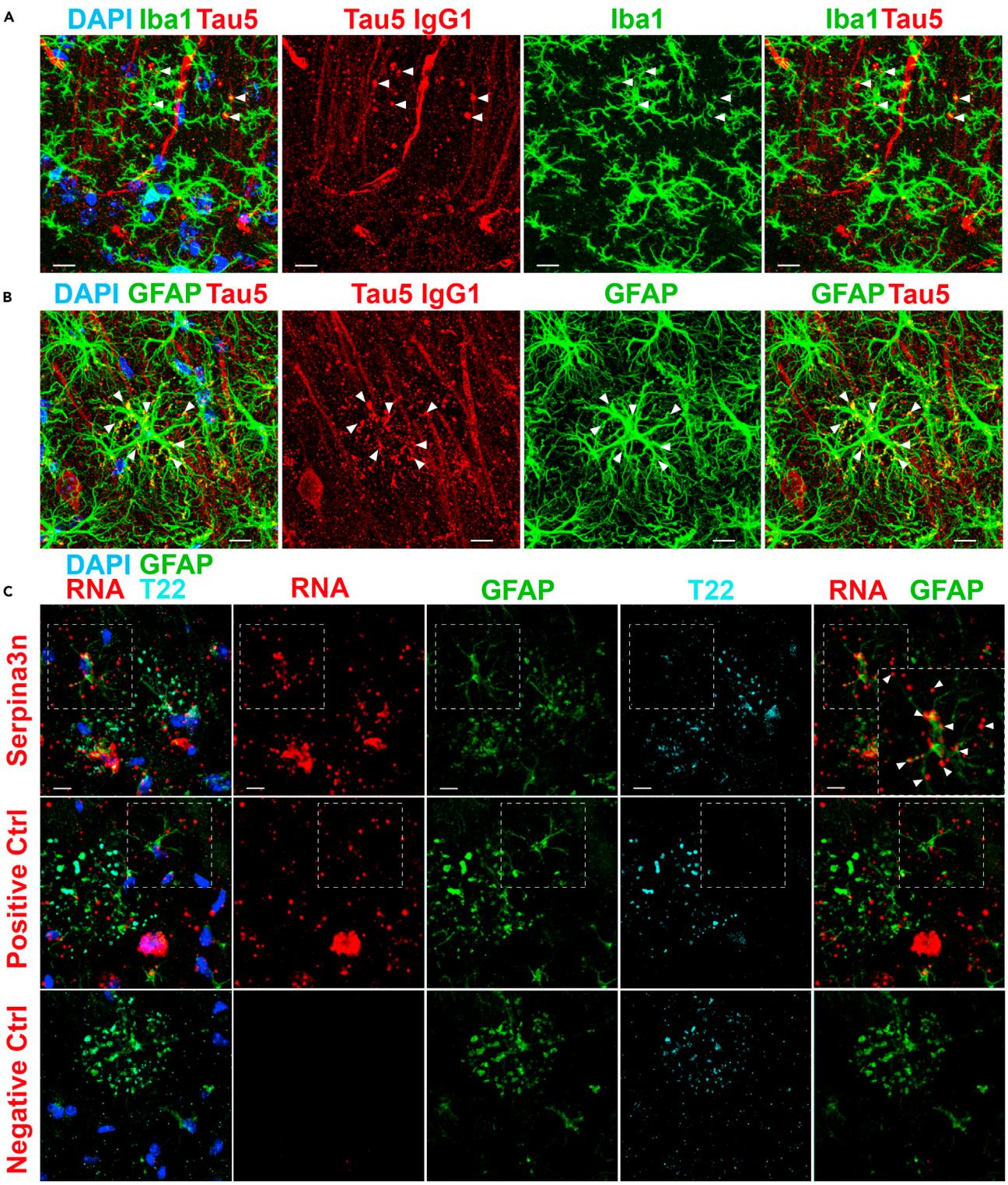

Figure 5. Tau-Immunoreactive Granules Are Associated with Reactive Astrocytes

(A) Immunofluorescent confocal images of aged (21-mo) 3xTg-AD mice show distal processes of microglia detected with anti-rabbit Iba1 (Iba1, green) that associate with and envelop anti-mouse IgG1-specific $tau5_{IR}$ granules (Tau5 IgG1, red) in the CA1 and SR of aged 3xTg-AD mice.

(B) Distal processes of astrocytes detected with anti-rabbit GFAP (GFAP, green) contain and envelop many anti-mouse IgG1-specific $tau5_{IR}$ granules (Tau5 IgG1, red) in the CA1 and SR of aged 3xTg-AD mice.

Figure 5. *Continued*

(C) Confocal images of dual *in situ* RNA labeling and immunofluorescence shows Serpina3n expression (red) in processes of reactive astrocytes (GFAP, green) entangled with T22-positive hippocampal clusters (T22, cyan). Robust expression of Ppib (positive control, red) is also detected in affected astrocytes (green) and other cells (DAPI, blue), whereas the negative control probe (red) is not detected in the hippocampus. Scale bars, 10 μm; arrowheads indicate sites of co-localization. See also Figure S5.

DISCUSSION

In this study, we characterized tau-1_{IR} clusters, which are highly reminiscent and overlapping with previously characterized PAS granules that accumulate predominantly in the aged mouse hippocampus. Using histology and molecular approaches, our results indicate that tau is a *bona fide* constituent of these granules in both mice and humans and that tau_{IR} granules represent a subset of an IgM-reactive pool that has not been defined in the literature. In contrast to more mature tau pathology in AD brain that is typically marked by phospho-tau immunoreactivity, our epitope profiling shows that hypo-phosphorylated, rather than hyper-phosphorylated tau, may be enriched within PAS granules and CA. Since hypo-phosphorylated tau species have been reported to precede subsequent tau hyper-phosphorylation (Liang et al., 2009, Lopresti and Konat, 2001), we propose that PAS granules may harbor a specific age-related conformational tau variant, which, given enough time, may evolve into more mature tau pathology. In light of our study showing that tau-1_{IR} cluster formation occurs in response to neuroinflammatory triggers (e.g., LPS exposure) (Tseng et al., 2017), CA and PAS granules could initially be generated in an attempt to clear tau and other aggregate-prone proteins but may then become stabilized in the aged brain, which could accelerate tau pathogenesis. The biochemical isolation of these structures, followed by mass spectrometry and other proteomics approaches, could identify PTM signatures that more fully characterize this particular tau strain.

We show that tau is present within some, but not all, human CA in control subjects and patients with AD. Our semi-quantitative CA rating has identified a potential negative correlation between tau-positive CA and severity of Braak staging (Figure S7). However, the precise role of CA throughout normal and pathological aging remains unclear, as additional studies are needed to determine whether CA correlates with one or more neuropathological, genetic, or cognitive variables that are linked to clinical disease onset or progression. We speculate that a particular tau strain may originate from CA, an exciting area for further research. Consistent with this possibility, our 3D reconstruction analysis indicates that anti-mouse IgG-specific neuritic tau may coalesce or merge with CA in human brain. The dome-like structures observed indicate that CA are "hollowed out" during antigen retrieval, which is supported by the observation that CA recovered from patient CSF lacks an outer membrane thought to be shed during the extrusion process into ventricular space (Riba et al., 2019). The same group analyzed CA in human tissue using a semithin sectioning approach and was able to capture the interior contents of CA, presumably by stabilizing the CA contents via epoxy resin per standard semithin sectioning procedures (Auge et al., 2019). Although our IHC results demonstrate that a total tau pool localizes within PAS granules and CA, we note that hyper-phosphorylated tau appeared to be restricted from these structures. The close proximity of hyper-phosphorylated tau around CA in AD brain may indicate that, upon exit from CA, tau could become subjected to pathological PTMs, including acetylation and phosphorylation, which may promote its aggregation and/or toxicity.

Previous studies have indicated that tau depletion is beneficial and protective against neuronal damage induced by Aβ pathology (Roberson et al., 2007), epileptic seizures (Devos et al., 2013, Gheyara et al., 2014; Holth et al., 2013; Li et al., 2014), and traumatic brain injury (TBI) (Cheng et al., 2014). Whether such neuroprotection is related to altered PAS granule accumulation is unclear. The reduction of PAS granules in TKO mice and increase in 6-month-old 3xTg-AD mice compared with age-matched controls suggests that tau could contribute to PAS granule stability; however, this possibility requires additional studies. Factors that regulate tau triage including HDAC6 and other autophagy regulators could also be linked to PAS granule formation or dissolution. In support of this possibility, we observed that loss of HDAC6 was sufficient to reduce PAS granules in aged mice (Tseng et al., 2017).

PAS granules and CA deposits increase with aging and are closely associated with astrocytes and microglia. Thus, we performed a more detailed evaluation of glia localization to PAS granules. Indeed, our data indicate that both microglia and, more prominently, astrocytes directly engage PAS granules. Given the steady decline of proteostasis during aging, it is plausible that aberrant glial activity in the aging brain coupled with declining autophagy and proteasome activity could exacerbate tau accumulation and drive chronic PAS granule formation. In fact, complete removal of tau (tau KO mice) was sufficient to eliminate anti-mouse IgG-specific tau antibody immunoreactivity and reduce the anti-mouse IgM-specific PAS

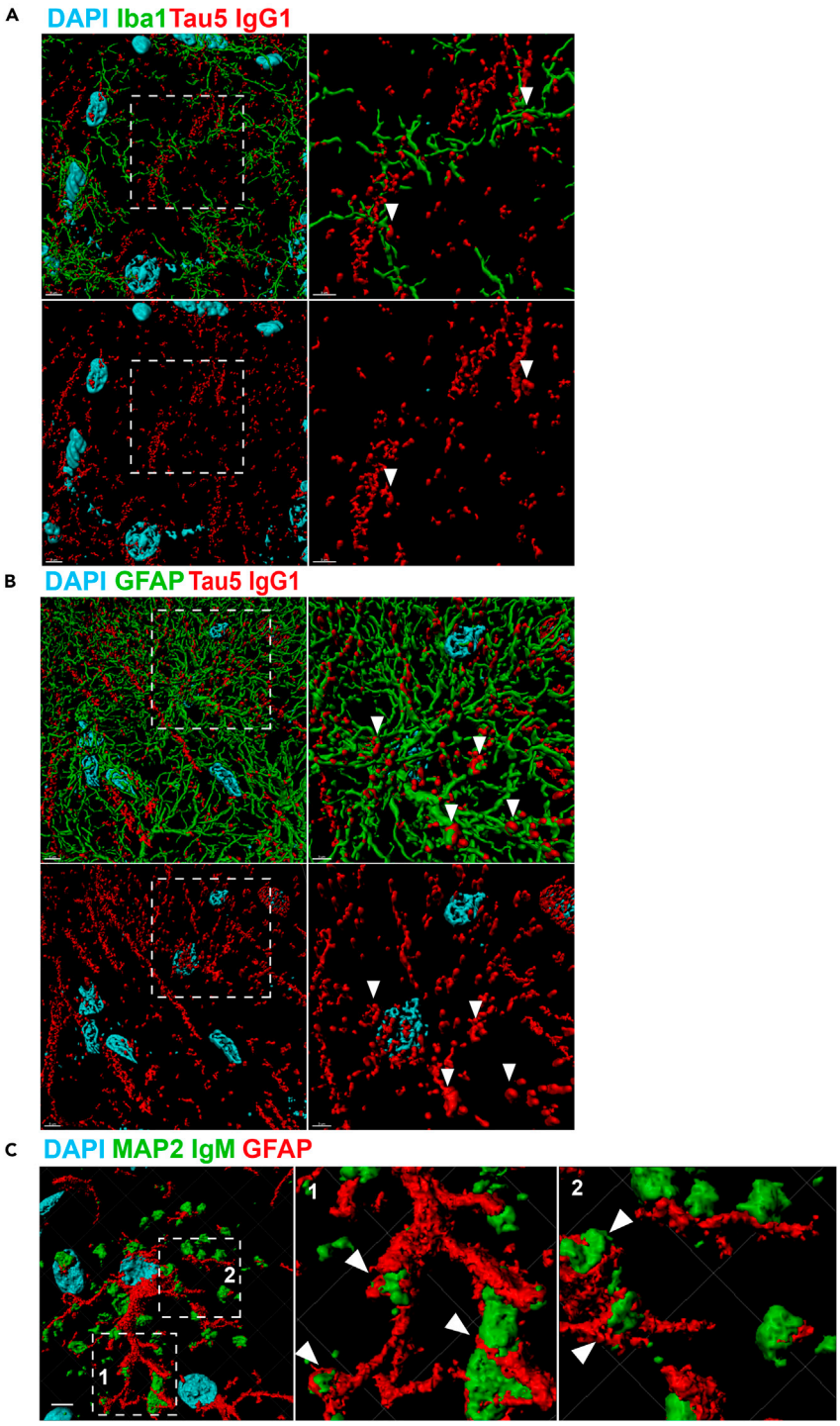

Figure 6. 3D Reconstruction of Tau-Immunoreactive Granules Reveals Extensive Association with Microglia and Astrocytes

(A) 3D reconstruction of confocal images obtained at 60x magnification (with 2× zoom) show that Iba1-positive microglial processes (green) associate with anti-mouse IgG-specific $tau5_{IR}$ dendrites and granules (Tau5 IgG1, red) in the SR of 3xTg-AD mice.

(B) 3D reconstruction shows that GFAP-positive astrocytic processes (green) associated with anti-mouse IgG-specific $tau5_{IR}$ dendrites and granules (Tau5 IgG1, red) in the SR of 3xTg-AD mice.

Figure 6. *Continued*
(C) 3D reconstruction shows that anti-mouse IgM-specific granules from the mouse monoclonal MAP2 primary antibody (MAP2 IgM, green) are closely juxtaposed along processes of GFAP-positive astrocytes (red). Scale bar, 5 μm (A, B, left); 3 μm (A, B, right); 5 μm (C, left). Arrowheads indicate regions of association.

granule pool by ~ 30% (Figures 2B and 2C), indicating that tau depletion could represent a strategy to suppress PAS granule or CA accumulation.

We used Serpina3n to mark reactive astrocytes since Serpina3n expression is sharply elevated after inflammatory stimuli (e.g., LPS injection) (Clarke et al., 2018). The transcriptional pattern of Serpina3n specifically in the hippocampus (Zhang et al., 2014b) is consistent with PAS granule accumulation and may be linked to an age-related increase in A1 neurotoxic astrocytes, which is common in neurodegenerative disorders such as AD or amyotrophic lateral sclerosis (ALS) characterized by complement-mediated synapse loss (Liddelow et al., 2017). Despite the strong correlation between toxic astrocytes and age-related neurodegeneration, little is known about the role of Serpina3n in aging or the pathophysiology of AD. Serpina3n, also commonly referred to as α-1-antichymotrypsin (ACT), is primarily expressed in mature astrocytes in humans (Zhang et al., 2016), is increased in AD patient brain, and also has been shown to promote abnormally modified tau in primary cortical neurons via the c-Jun N-terminal kinase pathway (Padmanabhan et al., 2006). Serpina3n/ACT is an irreversible inhibitor of chymotrypsin, a protease that cleaves tau between the N-terminal projection domain and the microtubule repeat domain (Steiner et al., 1990). Serpina3n-expressing reactive astrocytes may therefore exert neurotoxicity, in part, by impairing the degradation of tau and the clearance of PAS granules.

Our findings strengthen the notion that CA and PAS granules represent a marker of brain vulnerability during aging. CA1-localized astrocytes were reportedly more sensitive to oxidative stress compared with other brain regions (Ouyang et al., 2007), suggesting the CA1 region is particularly vulnerable to proteotoxic stress during aging. The marked association of PAS granules with reactive astrocytes implies that inflammation may trigger further downstream dysfunction during aging. For example, astrocytic endfeet associate with the vasculature in an aquaporin-dependent manner and the localization of aquaporins is increasingly dysregulated in response to brain injury and throughout the aging process (Mccaslin et al., 2011, Nielsen et al., 1997; Rash et al., 1998; Verbavatz et al., 1997). Therefore, chronically reactive astrocytes could impair the clearance of PAS granules or CA, disrupt glymphatic function, and potentially stabilize tau to promote its toxicity (Navarro et al., 2018).

Our observations support that astrocytes are intimately engaged with CA in human patients and PAS granules in aged rodents. The precise role of astrocyte reactivity in AD remains unclear, with some studies suggesting astrocytes are vital for neuronal survival in normal (Cui et al., 2001) and pathological conditions (Faulkner et al., 2004), yet exacerbate memory deficits in AD models (Wu et al., 2014). Astrocytes have also been observed clearing Aβ-positive presynaptic dystrophies in amyloid models (Gomez-Arboledas et al., 2018). Astrocyte reactivity in response to the hallmark pathological aggregates in AD may therefore initially represent a compensatory response that eventually becomes pathological.

Given the close association of neuritic tau and astrocytic processes surrounding CA, it is tempting to speculate that reactive astrocytes may accelerate the conversion of anti-mouse IgG-specific tau_{IR} granules into more mature tau pathology or even facilitate tau release and spread from the hippocampus to neocortical brain regions in a prion-like manner. In such a scenario, astrocytes, PAS granules, and CA could potentially play an unanticipated role in mediating tau stabilization, aggregation, and spreading in tauopathies, which could provide new and unanticipated avenues for therapeutic intervention. Conversely, PAS granules and CA may represent an attempt by phagocytic astrocytes to clear neuronal debris including those induced by age-related stress. Related to this point, our correlation analyses of CA-tau may indicate less tau localization to CA in the hippocampal sulcus during AD progression.

In summary, our findings describe a novel tau species in the aging brain and underscore the need to further investigate neuron-glia interactions throughout normal and pathological aging in both human patients and rodent models

Limitations of the Study

Our study demonstrates that tau within PAS granules and CA is predominantly de-phosphorylated at the tau-1 epitope. Future studies are needed to investigate other phospho-epitopes or post-translational

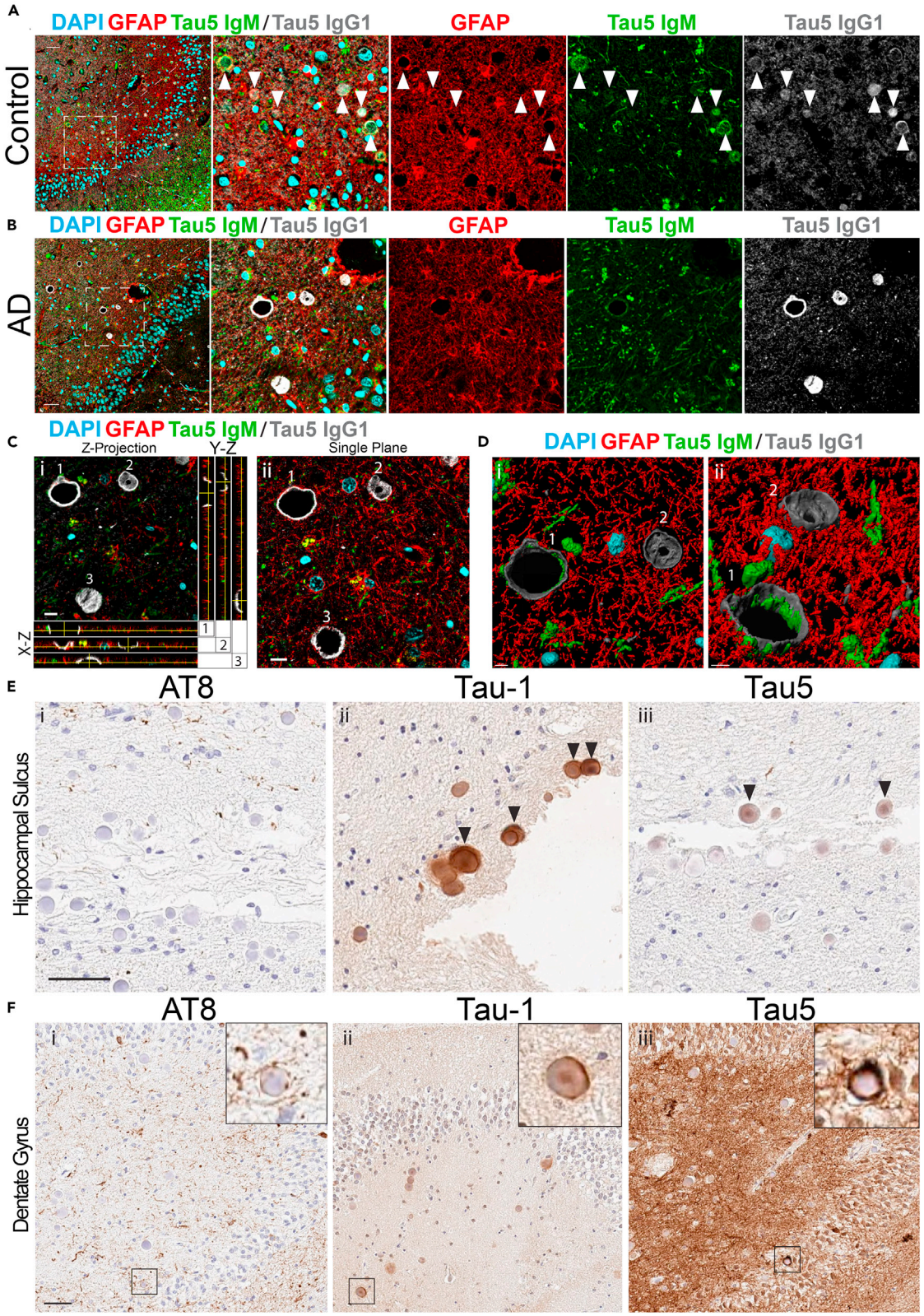
A
DAPI GFAP Tau5 IgM / Tau5 IgG1
GFAP
Tau5 IgM
Tau5 IgG1
Control
B
DAPI GFAP Tau5 IgM / Tau5 IgG1
GFAP
Tau5 IgM
Tau5 IgG1
AD
C
DAPI GFAP Tau5 IgM / Tau5 IgG1
Z-Projection
Y-Z
Single Plane
X-Z
D
DAPI GFAP Tau5 IgM / Tau5 IgG1
E
AT8
Tau-1
Tau5
Hippocampal Sulcus
F
AT8
Tau-1
Tau5
Dentate Gyrus

Figure 7. Tau-Immunoreactive CA in Human Control and AD Brain

(A) Confocal images of human control hippocampus immunostained with tau5 and GFAP primary antibodies and anti-mouse IgM μ-chain (Tau5 IgM, green), anti-rabbit (GFAP, red), and anti-mouse IgG1 γ-chain-specific (Tau5 IgG1, gray) secondary antibodies. Tau5 detects tau within CA when labeled with an anti-mouse IgG1 secondary antibody (gray). CA were labeled with an anti-mouse IgM μ-chain-specific secondary antibody (green). GFAP surrounds CA when labeled with anti-rabbit secondary antibody (red). Scale bar, 50 μm (arrowheads indicate immunoreactive CA).

(B) Confocal images of human AD hippocampus immunostained with tau5 and GFAP primary antibodies and isotype-specific secondaries detailed above. Tau5 detects tau within CA when labeled with an anti-mouse IgG1 secondary antibody (gray). CA were labeled with an anti-mouse IgM-specific secondary antibody (green). GFAP outlines but does not fill CA when labeled with an anti-rabbit secondary antibody (red). Scale bar, 50 μm.

(C) Average-intensity Z projection from selected region in (B), surrounded by orthogonal views targeted to individual CA labeled as 1, 2, and 3 (i). A single plane confocal image of AD patient hippocampus is also shown (ii). Scale bar, 10 μm.

(D) 3D reconstruction of inset showing hollowed structure of CA from (i) top-down and (ii) oblique angular view.

(E) Wide-field IHC images of the hippocampal sulcus in serial sections from an AD patient brain stained with (i) AT8, (ii) Tau-1, and (iii) Tau5 primary antibodies and anti-mouse IgG1-specific or anti-mouse IgG2a-specific HRP-conjugated secondary antibodies. Scale bar, 50 μm. Arrowheads indicate tau-immunoreactive CA.

(F) Wide-field IHC images of the dentate gyrus in serial sections from AD patient brain stained with (i) AT8, (ii) tau-1, and (iii) tau5 primary antibodies and detected with anti-mouse IgG1-specific or anti-mouse IgG2a-specific HRP-conjugated secondary antibodies. Scale bar, 50 μm.

See also Figures S6 and S7 and Table S3.

modifications that may alter tau's localization to PAS granules or CA. Our experiments do not address the question of whether PAS granules or CA are protective or rather act as potential pathological features of aging. Although our studies indicate that tau localizes to these structures, they may not be completely synonymous between mouse and human species, and therefore the species-specific consequences of tau localization to PAS granules and CA requires further investigation.

Resource Availability

Lead Contact

Further information and requests for resources and reagents should be directed to and will be fulfilled by the Lead Contact, Todd J. Cohen (toddcohen@neurology.unc.edu).

Materials Availability

This study did not generate unique reagents.

Data and Code Availability

Data in this study will be provided upon request from the corresponding author.

METHODS

All methods can be found in the accompanying Transparent Methods supplemental file.

SUPPLEMENTAL INFORMATION

Supplemental Information can be found online at https://doi.org/10.1016/j.isci.2020.101255.

ACKNOWLEDGMENTS

Support for this work was provided by National Institutes of Health (NIH) grants R01AG061188 (T.J.C) and R21AG058080 (T.J.C.), the National Center for Advancing Translational Sciences (NCATS) grant UL1TR001111 (T.J.C.), Alzheimer's Association grant NIRG-14-321219 (T.J.C.), an Association for Frontotemporal Degeneration (AFTD) pilot grant (T.J.C.), and the American Federation for Aging Research (AFAR) grant RAG15247 (T.J.C.). Microscopy was performed at the UNC Neuroscience Microscopy Core Facility supported by grant P30NS045892 and the NIH-NICHD Intellectual and Developmental Disabilities Research Center Support grant U54HD079124. The content is solely the responsibility of the authors and does not necessarily represent the official views of the National Institutes of Health. We thank Dr. John Trojanowski from the Center for Neurodegenerative Disease Research (CNDR) at the University of Pennsylvania for providing human postmortem control and AD brain tissue along with their patient demographics.

AUTHOR CONTRIBUTIONS

C.M.W. performed most of the experiments in this study. A.A. assisted with immunoblotting, whereas J.-H.T., R.M., S.S., H.A., and S.T. assisted with immunofluorescence staining, tissue sectioning, and confocal microscopy. J.S., R.M., S.S., and Y.-Y.I.S. assisted with data analysis and data interpretation. D.J.I. and R.L.

performed IHC analysis of human postmortem brain tissues and imaging. C.M.W. and T.J.C. wrote the manuscript. This study was directed and supervised by T.J.C.

DECLARATION OF INTERESTS

The authors declare no competing interests.

Received: March 10, 2020
Revised: May 19, 2020
Accepted: June 5, 2020
Published: July 24, 2020

REFERENCES

Akiyama, H., Kameyama, M., Akiguchi, I., Sugiyama, H., Kawamata, T., Fukuyama, H., Kimura, H., Matsushita, M., and Takeda, T. (1986). Periodic acid-Schiff (PAS)-positive, granular structures increase in the brain of senescence accelerated mouse (SAM). Acta Neuropathol. *72*, 124–129.

Auge, E., Bechmann, I., Llor, N., Vilaplana, J., Krueger, M., and Pelegri, C. (2019). Corpora amylacea in human hippocampal brain tissue are intracellular bodies that exhibit a homogeneous distribution of neo-epitopes. Sci. Rep. *9*, 2063.

Auge, E., Cabezon, I., Pelegri, C., and Vilaplana, J. (2017). New perspectives on corpora amylacea in the human brain. Sci. Rep. *7*, 41807.

Auge, E., Duran, J., Guinovart, J.J., Pelegri, C., and Vilaplana, J. (2018). Exploring the elusive composition of corpora amylacea of human brain. Sci. Rep. *8*, 13525.

Baker, C., Belbin, O., Kalsheker, N., and Morgan, K. (2007). SERPINA3 (aka alpha-1-antichymotrypsin). Front. Biosci. *12*, 2821–2835.

Binder, L.I., Frankfurter, A., and Rebhun, L.I. (1985). The distribution of tau in the mammalian central nervous system. J. Cell Biol. *101*, 1371–1378.

Cana, A., Herder, V., Hansmann, F., Beineke, A., Baumgartner, W., and Spitzbarth, I. (2015). Characterization of periodic acid-schiff-positive granular deposits in the Hippocampus of SJL/J mice. Toxicol. Pathol. *43*, 737–742.

Chen, Z., Jalabi, W., Hu, W., Park, H.J., Gale, J.T., Kidd, G.J., Bernatowicz, R., Gossman, Z.C., Chen, J.T., Dutta, R., and Trapp, B.D. (2014). Microglial displacement of inhibitory synapses provides neuroprotection in the adult brain. Nat. Commun. *5*, 4486.

Cheng, J.S., Craft, R., Yu, G.Q., Ho, K., Wang, X., Mohan, G., Mangnitsky, S., Ponnusamy, R., and Mucke, L. (2014). Tau reduction diminishes spatial learning and memory deficits after mild repetitive traumatic brain injury in mice. PLoS One *9*, e115765.

Clarke, L.E., Liddelow, S.A., Chakraborty, C., Munch, A.E., Heiman, M., and Barres, B.A. (2018). Normal aging induces A1-like astrocyte reactivity. Proc. Natl. Acad. Sci. U S A *115*, E1896–E1905.

Cohen, T.J., Guo, J.L., Hurtado, D.E., Kwong, L.K., Mills, I.P., Trojanowski, J.Q., and Lee, V.M. (2011). The acetylation of tau inhibits its function and promotes pathological tau aggregation. Nat. Commun. *2*, 252.

Cui, W., Allen, N.D., Skynner, M., Gusterson, B., and Clark, A.J. (2001). Inducible ablation of astrocytes shows that these cells are required for neuronal survival in the adult brain. Glia *34*, 272–282.

Devos, S.L., Goncharoff, D.K., Chen, G., Kebodeaux, C.S., Yamada, K., Stewart, F.R., Schuler, D.R., Maloney, S.E., Wozniak, D.F., Rigo, F., et al. (2013). Antisense reduction of tau in adult mice protects against seizures. J. Neurosci. *33*, 12887–12897.

Doehner, J., Madhusudan, A., Konietzko, U., Fritschy, J.M., and Knuesel, I. (2010). Co-localization of Reelin and proteolytic AbetaPP fragments in hippocampal plaques in aged wild-type mice. J. Alzheimers Dis. *19*, 1339–1357.

Drewes, G., Ebneth, A., Preuss, U., Mandelkow, E.M., and Mandelkow, E. (1997). MARK, a novel family of protein kinases that phosphorylate microtubule-associated proteins and trigger microtubule disruption. Cell *89*, 297–308.

Faulkner, J.R., Herrmann, J.E., Woo, M.J., Tansey, K.E., Doan, N.B., and Sofroniew, M.V. (2004). Reactive astrocytes protect tissue and preserve function after spinal cord injury. J. Neurosci. *24*, 2143–2155.

Gheyara, A.L., Ponnusamy, R., Djukic, B., Craft, R.J., Ho, K., Guo, W., Finucane, M.M., Sanchez, P.E., and Mucke, L. (2014). Tau reduction prevents disease in a mouse model of Dravet syndrome. Ann. Neurol. *76*, 443–456.

Gomez-Arboledas, A., Davila, J.C., Sanchez-Mejias, E., Navarro, V., Nunez-Diaz, C., Sanchez-Varo, R., Sanchez-Mico, M.V., Trujillo-Estrada, L., Fernandez-Valenzuela, J.J., Vizuete, M., et al. (2018). Phagocytic clearance of presynaptic dystrophies by reactive astrocytes in Alzheimer's disease. Glia *66*, 637–653.

Holth, J.K., Bomben, V.C., Reed, J.G., Inoue, T., Younkin, L., Younkin, S.G., Pautler, R.G., Botas, J., and Noebels, J.L. (2013). Tau loss attenuates neuronal network hyperexcitability in mouse and Drosophila genetic models of epilepsy. J. Neurosci. *33*, 1651–1659.

Jucker, M., Walker, L.C., Schwarb, P., Hengemihle, J., Kuo, H., Snow, A.D., Bamert, F., and Ingram, D.K. (1994). Age-related deposition of glia-associated fibrillar material in brains of C57BL/6 mice. Neuroscience *60*, 875–889.

Knuesel, I., Nyffeler, M., Mormede, C., Muhia, M., Meyer, U., Pietropaolo, S., Yee, B.K., Pryce, C.R., Laferla, F.M., Marighetto, A., and Feldon, J. (2009). Age-related accumulation of Reelin in amyloid-like deposits. Neurobiol. Aging *30*, 697–716.

Kuo, H., Ingram, D.K., Walker, L.C., Tian, M., Hengemihle, J.M., and Jucker, M. (1996). Similarities in the age-related hippocampal deposition of periodic acid-schiff-positive granules in the senescence-accelerated mouse P8 and C57BL/6 mouse strains. Neuroscience *74*, 733–740.

Lasagna-Reeves, C.A., Castillo-Carranza, D.L., Sengupta, U., Sarmiento, J., Troncoso, J., Jackson, G.R., and Kayed, R. (2012). Identification of oligomers at early stages of tau aggregation in Alzheimer's disease. FASEB J. *26*, 1946–1959.

Li, Z., Hall, A.M., Kelinske, M., and Roberson, E.D. (2014). Seizure resistance without parkinsonism in aged mice after tau reduction. Neurobiol. Aging *35*, 2617–2624.

Liang, Z., Liu, F., Iqbal, K., Grundke-Iqbal, I., and Gong, C.X. (2009). Dysregulation of tau phosphorylation in mouse brain during excitotoxic damage. J. Alzheimers Dis. *17*, 531–539.

Libard, S., Popova, S.N., Amini, R.M., Karja, V., Pietilainen, T., Hamalainen, K.M., Sundstrom, C., Hesselager, G., Bergqvist, M., Ekman, S., et al. (2014). Human cytomegalovirus tegument protein pp65 is detected in all intra- and extra-axial brain tumours independent of the tumour type or grade. PLoS One *9*, e108861.

Liddelow, S.A., Guttenplan, K.A., Clarke, L.E., Bennett, F.C., Bohlen, C.J., Schirmer, L., Bennett, M.L., Munch, A.E., Chung, W.S., Peterson, T.C., et al. (2017). Neurotoxic reactive astrocytes are induced by activated microglia. Nature *541*, 481–487.

Lopresti, P., and Konat, G.W. (2001). Hydrogen peroxide induces transient dephosphorylation of tau protein in cultured rat oligodendrocytes. Neurosci. Lett. *311*, 142–144.

Madhusudan, A., Sidler, C., and Knuesel, I. (2009). Accumulation of reelin-positive plaques is accompanied by a decline in basal forebrain projection neurons during normal aging. Eur. J. Neurosci. *30*, 1064–1076.

Maeda, S., Sahara, N., Saito, Y., Murayama, S., Ikai, A., and Takashima, A. (2006). Increased levels

of granular tau oligomers: an early sign of brain aging and Alzheimer's disease. Neurosci. Res. *54*, 197–201.

Manich, G., Auge, E., Cabezon, I., Pallas, M., Vilaplana, J., and Pelegri, C. (2015). Neo-epitopes emerging in the degenerative hippocampal granules of aged mice can be recognized by natural IgM auto-antibodies. Immun. Ageing *12*, 23.

Manich, G., Cabezon, I., Auge, E., Pelegri, C., and Vilaplana, J. (2016). Periodic acid-Schiff granules in the brain of aged mice: from amyloid aggregates to degenerative structures containing neo-epitopes. Ageing Res. Rev. *27*, 42–55.

Manich, G., Cabezon, I., Camins, A., Pallas, M., Liberski, P.P., Vilaplana, J., and Pelegri, C. (2014a). Clustered granules present in the hippocampus of aged mice result from a degenerative process affecting astrocytes and their surrounding neuropil. Age (Dordr) *36*, 9690.

Manich, G., Del Valle, J., Cabezon, I., Camins, A., Pallas, M., Pelegri, C., and Vilaplana, J. (2014b). Presence of a neo-epitope and absence of amyloid beta and tau protein in degenerative hippocampal granules of aged mice. Age (Dordr) *36*, 151–165.

Mccaslin, A.F., Chen, B.R., Radosevich, A.J., Cauli, B., and Hillman, E.M. (2011). In vivo 3D morphology of astrocyte-vasculature interactions in the somatosensory cortex: implications for neurovascular coupling. J. Cereb. Blood Flow Metab. *31*, 795–806.

Mitsuno, S., Takahashi, M., Gondo, T., Hoshii, Y., Hanai, N., Ishihara, T., and Yamada, M. (1999). Immunohistochemical, conventional and immunoelectron microscopical characteristics of periodic acid-Schiff-positive granules in the mouse brain. Acta Neuropathol. *98*, 31–38.

Nakamura, S., Akiguchi, I., Seriu, N., Ohnishi, K., Takemura, M., Ueno, M., Tomimoto, H., Kawamata, T., Kimura, J., and Hosokawa, M. (1995). Monoamine oxidase-B-positive granular structures in the hippocampus of aged senescence-accelerated mouse (SAMP8). Acta Neuropathol. *90*, 626–632.

Navarro, P.P., Genoud, C., Castano-Diez, D., Graff-Meyer, A., Lewis, A.J., De Gier, Y., Lauer, M.E., Britschgi, M., Bohrmann, B., Frank, S., et al. (2018). Cerebral Corpora amylacea are dense membranous labyrinths containing structurally preserved cell organelles. Sci. Rep. *8*, 18046.

Nielsen, S., Nagelhus, E.A., Amiry-Moghaddam, M., Bourque, C., Agre, P., and Ottersen, O.P. (1997). Specialized membrane domains for water transport in glial cells: high-resolution immunogold cytochemistry of aquaporin-4 in rat brain. J. Neurosci. *17*, 171–180.

Oddo, S., Caccamo, A., Shepherd, J.D., Murphy, M.P., Golde, T.E., Kayed, R., Metherate, R., Mattson, M.P., Akbari, Y., and Laferla, F.M. (2003). Triple-transgenic model of Alzheimer's disease with plaques and tangles: intracellular Abeta and synaptic dysfunction. Neuron *39*, 409–421.

Ouyang, Y.B., Voloboueva, L.A., Xu, L.J., and Giffard, R.G. (2007). Selective dysfunction of hippocampal CA1 astrocytes contributes to delayed neuronal damage after transient forebrain ischemia. J. Neurosci. *27*, 4253–4260.

Padmanabhan, J., Levy, M., Dickson, D.W., and Potter, H. (2006). Alpha1-antichymotrypsin, an inflammatory protein overexpressed in Alzheimer's disease brain, induces tau phosphorylation in neurons. Brain *129*, 3020–3034.

Pisa, D., Alonso, R., Marina, A.I., Rabano, A., and Carrasco, L. (2018). Human and microbial proteins from corpora amylacea of Alzheimer's disease. Sci. Rep. *8*, 9880.

Pisa, D., Alonso, R., Rabano, A., and Carrasco, L. (2016). Corpora amylacea of brain tissue from neurodegenerative diseases are stained with specific antifungal antibodies. Front Neurosci. *10*, 86.

Porquet, D., Casadesus, G., Bayod, S., Vicente, A., Canudas, A.M., Vilaplana, J., Pelegri, C., Sanfeliu, C., Camins, A., Pallas, M., and Del Valle, J. (2013). Dietary resveratrol prevents Alzheimer's markers and increases life span in SAMP8. Age (Dordr) *35*, 1851–1865.

Puzzo, D., Gulisano, W., Palmeri, A., and Arancio, O. (2015). Rodent models for Alzheimer's disease drug discovery. Expert Opin. Drug Discov. *10*, 703–711.

Rash, J.E., Yasumura, T., Hudson, C.S., Agre, P., and Nielsen, S. (1998). Direct immunogold labeling of aquaporin-4 in square arrays of astrocyte and ependymocyte plasma membranes in rat brain and spinal cord. Proc. Natl. Acad. Sci. U S A. *95*, 11981–11986.

Riba, M., Auge, E., Campo-Sabariz, J., Moral-Anter, D., Molina-Porcel, L., Ximelis, T., Ferrer, R., Martin-Venegas, R., Pelegri, C., and Vilaplana, J. (2019). Corpora amylacea act as containers that remove waste products from the brain. Proc. Natl. Acad. Sci. U S A. *116*, 26038–26048.

Roberson, E.D., Scearce-Levie, K., Palop, J.J., Yan, F., Cheng, I.H., Wu, T., Gerstein, H., Yu, G.Q., and Mucke, L. (2007). Reducing endogenous tau ameliorates amyloid beta-induced deficits in an Alzheimer's disease mouse model. Science *316*, 750–754.

Robertson, T.A., Dutton, N.S., Martins, R.N., Roses, A.D., Kakulas, B.A., and Papadimitriou, J.M. (1998). Age-related congophilic inclusions in the brains of apolipoprotein E-deficient mice. Neuroscience *82*, 171–180.

Selenica, M.L., Benner, L., Housley, S.B., Manchec, B., Lee, D.C., Nash, K.R., Kalin, J., Bergman, J.A., Kozikowski, A., Gordon, M.N., and Morgan, D. (2014). Histone deacetylase 6 inhibition improves memory and reduces total tau levels in a mouse model of tau deposition. Alzheimers Res. Ther. *6*, 12.

Singhrao, S.K., Neal, J.W., and Newman, G.R. (1993). Corpora amylacea could be an indicator of neurodegeneration. Neuropathol. Appl. Neurobiol. *19*, 269–276.

Steiner, B., Mandelkow, E.M., Biernat, J., Gustke, N., Meyer, H.E., Schmidt, B., Mieskes, G., Soling, H.D., Drechsel, D., Kirschner, M.W., et al. (1990). Phosphorylation of microtubule-associated protein tau: identification of the site for Ca2(+)-calmodulin dependent kinase and relationship with tau phosphorylation in Alzheimer tangles. EMBO J. *9*, 3539–3544.

Szendrei, G.I., Lee, V.M., and Otvos, L., Jr. (1993). Recognition of the minimal epitope of monoclonal antibody Tau-1 depends upon the presence of a phosphate group but not its location. J. Neurosci. Res. *34*, 243–249.

Tseng, J.H., Xie, L., Song, S., Xie, Y., Allen, L., Ajit, D., Hong, J.S., Chen, X., Meeker, R.B., and Cohen, T.J. (2017). The deacetylase HDAC6 mediates endogenous neuritic tau pathology. Cell Rep. *20*, 2169–2183.

Vanni, S., Moda, F., Zattoni, M., Bistaffa, E., De Cecco, E., Rossi, M., Giaccone, G., Tagliavini, F., Haik, S., Deslys, J.P., et al. (2017). Differential overexpression of SERPINA3 in human prion diseases. Sci. Rep. *7*, 15637.

Verbavatz, J.M., Ma, T., Gobin, R., and Verkman, A.S. (1997). Absence of orthogonal arrays in kidney, brain and muscle from transgenic knockout mice lacking water channel aquaporin-4. J. Cell Sci. *110* (Pt 22), 2855–2860.

Wirak, D.O., Bayney, R., Ramabhadran, T.V., Fracasso, R.P., Hart, J.T., Hauer, P.E., Hsiau, P., Pekar, S.K., Scangos, G.A., Trapp, B.D., et al. (1991). Deposits of amyloid beta protein in the central nervous system of transgenic mice. Science *253*, 323–325.

Wu, Z., Guo, Z., Gearing, M., and Chen, G. (2014). Tonic inhibition in dentate gyrus impairs long-term potentiation and memory in an Alzheimer's [corrected] disease model. Nat. Commun. *5*, 4159.

Zhang, L., Liu, C., Wu, J., Tao, J.J., Sui, X.L., Yao, Z.G., Xu, Y.F., Huang, L., Zhu, H., Sheng, S.L., and Qin, C. (2014a). Tubastatin A/ACY-1215 improves cognition in Alzheimer's disease transgenic mice. J. Alzheimers Dis. *41*, 1193–1205.

Zhang, Y., Chen, K., Sloan, S.A., Bennett, M.L., Scholze, A.R., O'keeffe, S., Phatnani, H.P., Guarnieri, P., Caneda, C., Ruderisch, N., et al. (2014b). An RNA-sequencing transcriptome and splicing database of glia, neurons, and vascular cells of the cerebral cortex. J. Neurosci. *34*, 11929–11947.

Zhang, Y., Sloan, S.A., Clarke, L.E., Caneda, C., Plaza, C.A., Blumenthal, P.D., Vogel, H., Steinberg, G.K., Edwards, M.S., Li, G., et al. (2016). Purification and characterization of progenitor and mature human astrocytes Reveals transcriptional and functional differences with mouse. Neuron *89*, 37–53.

iScience, Volume *23*

Supplemental Information

The Accumulation of Tau-Immunoreactive Hippocampal Granules and Corpora Amylacea Implicates Reactive Glia in Tau Pathogenesis during Aging

Connor M. Wander, Jui-Heng Tseng, Sheng Song, Heba A. Al Housseiny, Dalton S. Tart, Aditi Ajit, Yen-Yu Ian Shih, Rebecca Lobrovich, Juan Song, Rick B. Meeker, David J. Irwin, and Todd J. Cohen

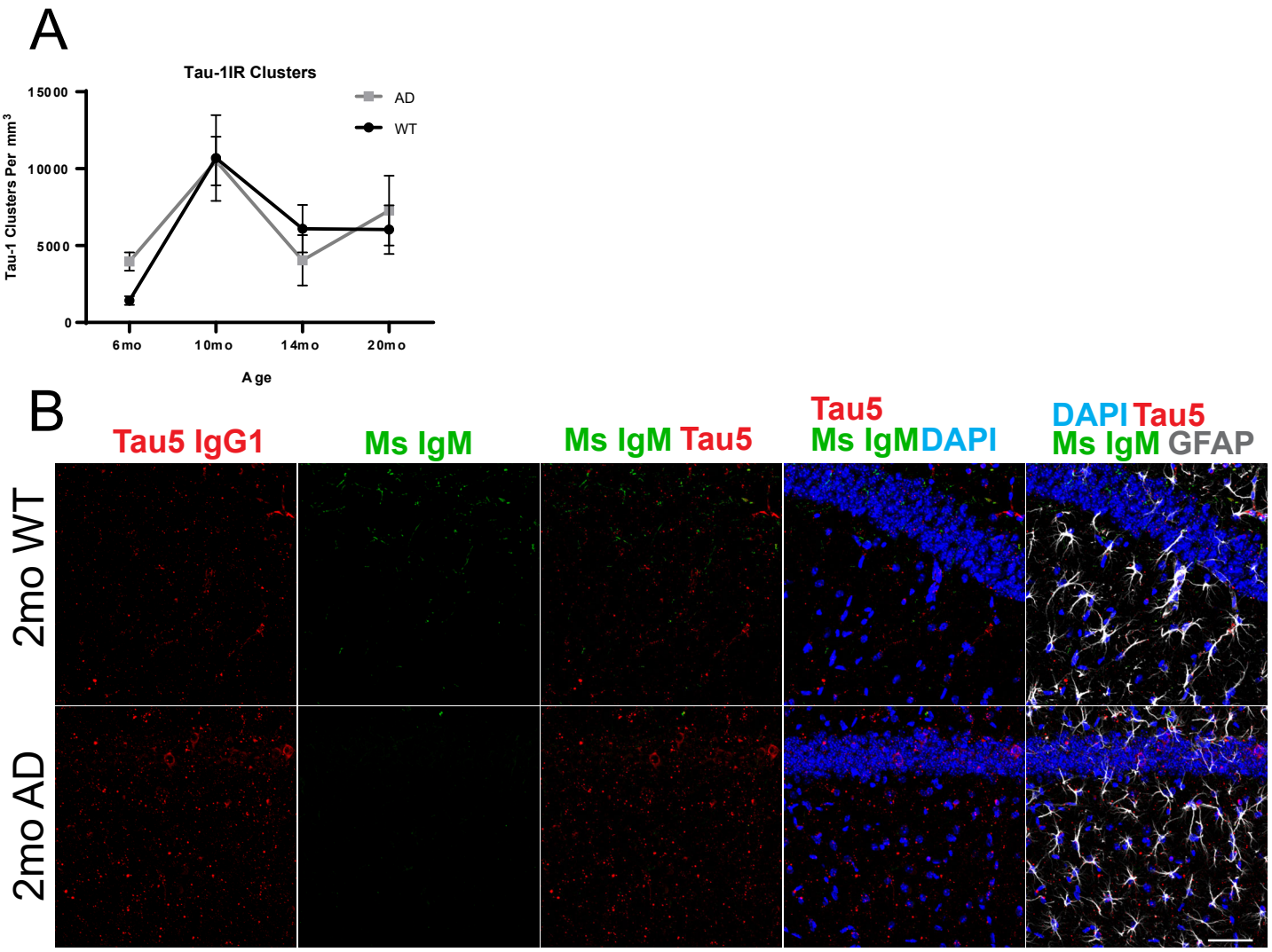

Figure S1. Tau cluster quantification in young and aged wild-type and 3xTg-AD animals, Related to Figure 1

(A) Quantification of tau-1 immunoreactive clusters detected with non-specific anti-mouse secondary antibodies in both aged 3xTg-AD (AD) and wild-type control (WT) mice. (B) Representative confocal images of hippocampi from 2mo WT and AD mice immunostained with tau5 and GFAP and labeled with anti-mouse IgM μ-chain specific (Ms IgM, green), anti-mouse IgG1 (Tau5 IgG1, red), and anti-rabbit IgG (GFAP, grey) secondary antibodies. Scale bar = 50 μm.

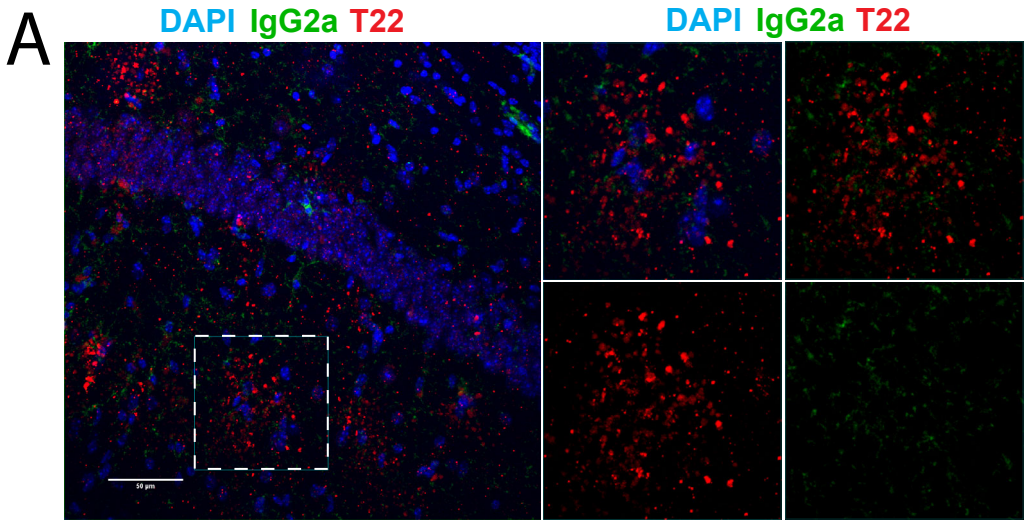

Figure S2. Isotype-specific control antibody validation, Related to Figure 2
(A) Confocal image of aged (21mo) 3xTg-AD mouse hippocampus immunostained with T22 in parallel with the anti-IgG2a isotype control antibody, conjugated with donkey anti-rabbit and anti-mouse secondary antibodies. T22 reliably detects PAS granules, which are not detected by the anti-IgG2a control antibody. Scale bar = 50 µm.

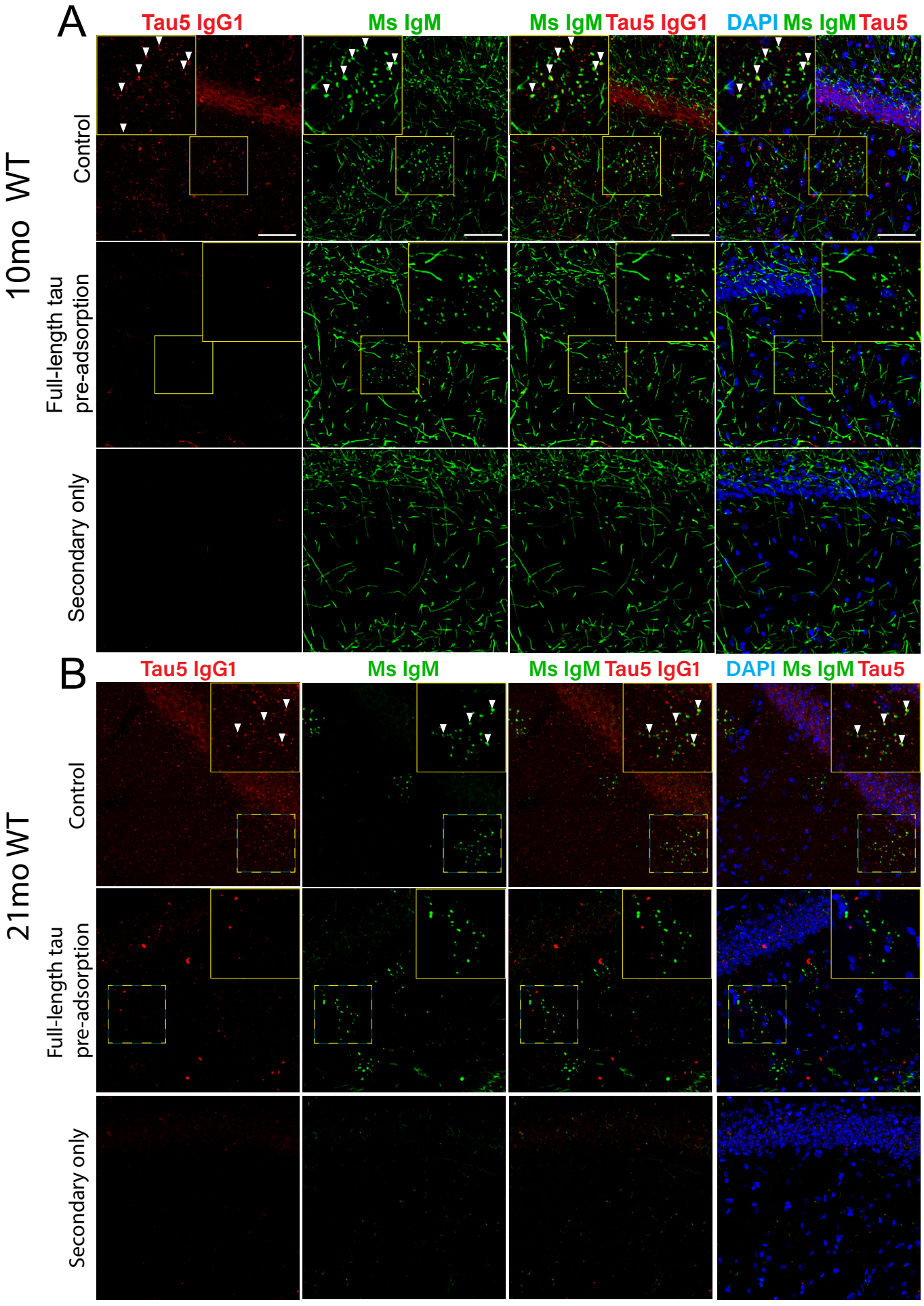
A
Tau5 IgG1
Ms IgM
Ms IgM Tau5 IgG1
DAPI Ms IgM Tau5
10mo WT
Control
Full-length tau pre-adsorption
Secondary only
B
Tau5 IgG1
Ms IgM
Ms IgM Tau5 IgG1
DAPI Ms IgM Tau5
21mo WT
Control
Full-length tau pre-adsorption
Secondary only

Figure S3. Analysis of tau clusters following epitope neutralization by immunoadsorption in aged wild-type animals, Related to Figure 3

(A) Immunofluorescent confocal images of the CA1 of middle-aged wild-type control animals (10mo WT) immunostained with tau5 and labeled with anti-mouse IgM μ-chain specific (Ms IgM, green) and anti-mouse IgG1 specific (Tau5 IgG1, red) secondary antibodies. Tau5 anti-mouse IgG1 specific signal (Tau5 IgG1, red) is sharply reduced in pre-adsorbed samples, whereas the anti-mouse IgM μ-chain specific (Ms IgM, green) signal remains. (B) Immunofluorescent confocal images of the CA1 of aged wild-type control animals (21mo WT) immunostained with tau5 and labeled with anti-mouse IgM μ-chain specific (Ms IgM, green) and anti-mouse IgG1 specific (Tau5 IgG1, red) secondary antibodies. Tau5 anti-mouse IgG1 specific signal (Tau5 IgG1, red) is sharply reduced in pre-adsorbed samples, whereas the anti-mouse IgM μ-chain specific (Ms IgM, green) signal remains. Arrowheads indicate prominent co-localization of anti-mouse IgG1 specific signal within tau5 granules immunoreactive to anti-mouse IgM μ-chain specific antibodies. Scale bar = 50 μm.

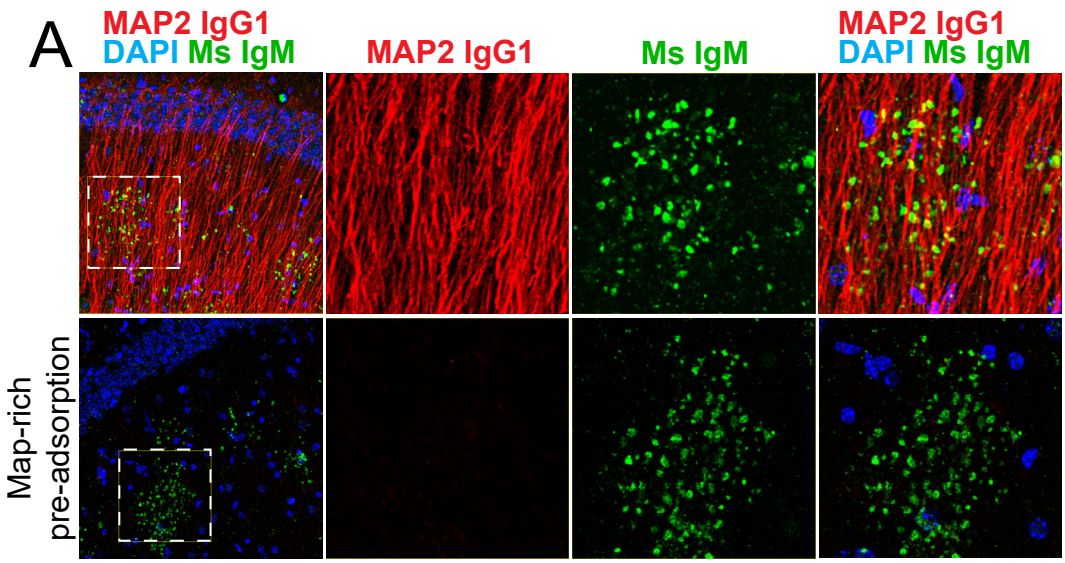

Figure S4. MAP2 antibody isotype validation, Related to Figure 4
(A) Immunofluorescent confocal image of the CA1 and SR of an aged (21mo) 3xTg-AD mouse stained by monoclonal MAP2 and labeled with goat anti-mouse IgM μ-chain specific secondary antibody (green) and an anti-mouse IgG1 γ-chain specific secondary (red) showing that MAP2 anti-mouse IgG1-specific immunoreactivity is not present in PAS granules. MAP2 anti-mouse IgG1-specific signal is eliminated by the co-incubation with a MAP-rich fraction (MRF), while the MAP2 anti-IgM signal (green) remains.

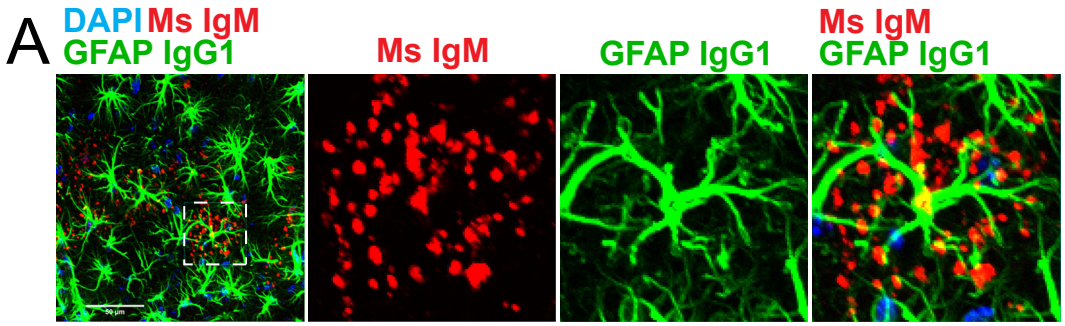

Figure S5. GFAP antibody isotype validation, Related to Figure 5
(A) Immunofluorescent confocal image of the CA1 and SR of an aged (21mo) 3xTg-AD mouse stained by monoclonal GFAP (Abcam) and detected with anti-mouse IgG1-specific (green) and anti-mouse IgM-specific (red) specific secondary antibodies. Scale bar = 50 μm.

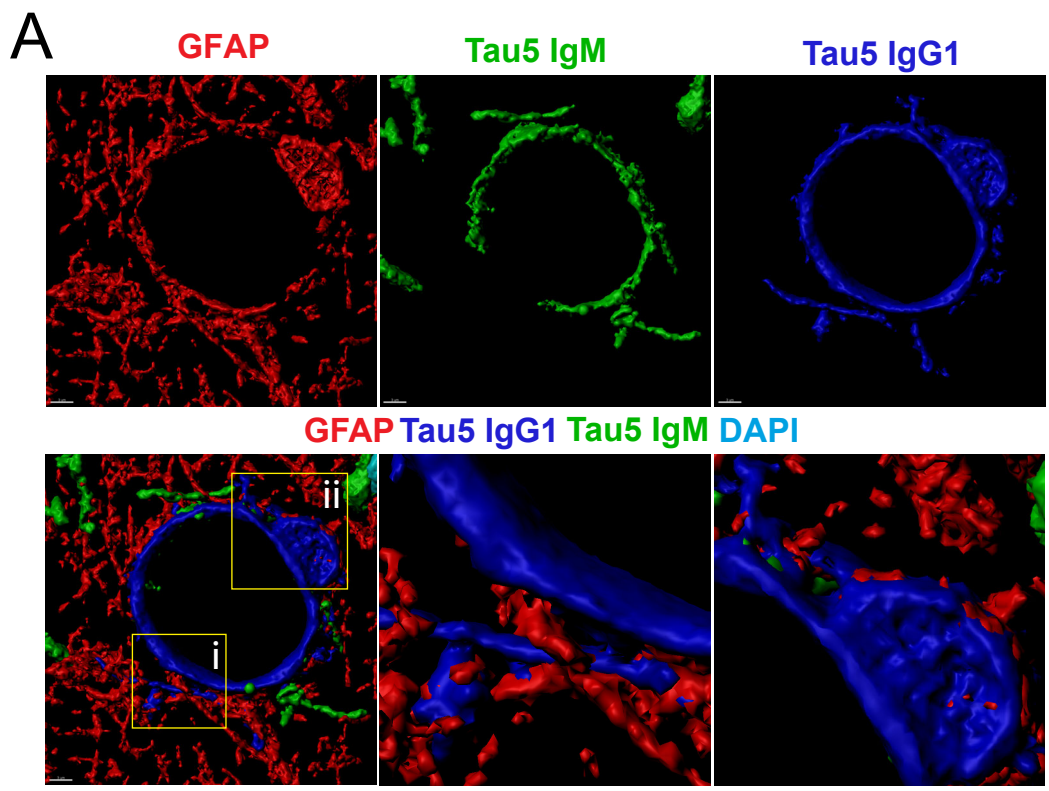

Figure S6. Tau-immunoreactive CA in association with neighboring astrocytes, Related to Figure 7

(A) A 3D reconstruction of a 60x confocal image of a human AD hippocampus (dentate granule layer) stained with tau5 and GFAP primary antibodies and detected with anti-mouse IgM μ-chain specific (Tau5 IgM, green), anti-mouse IgG1-specific (Tau5 IgG1, blue) and anti-rabbit IgG (GFAP, red) secondary antibodies. Scale bar = 3 μm.

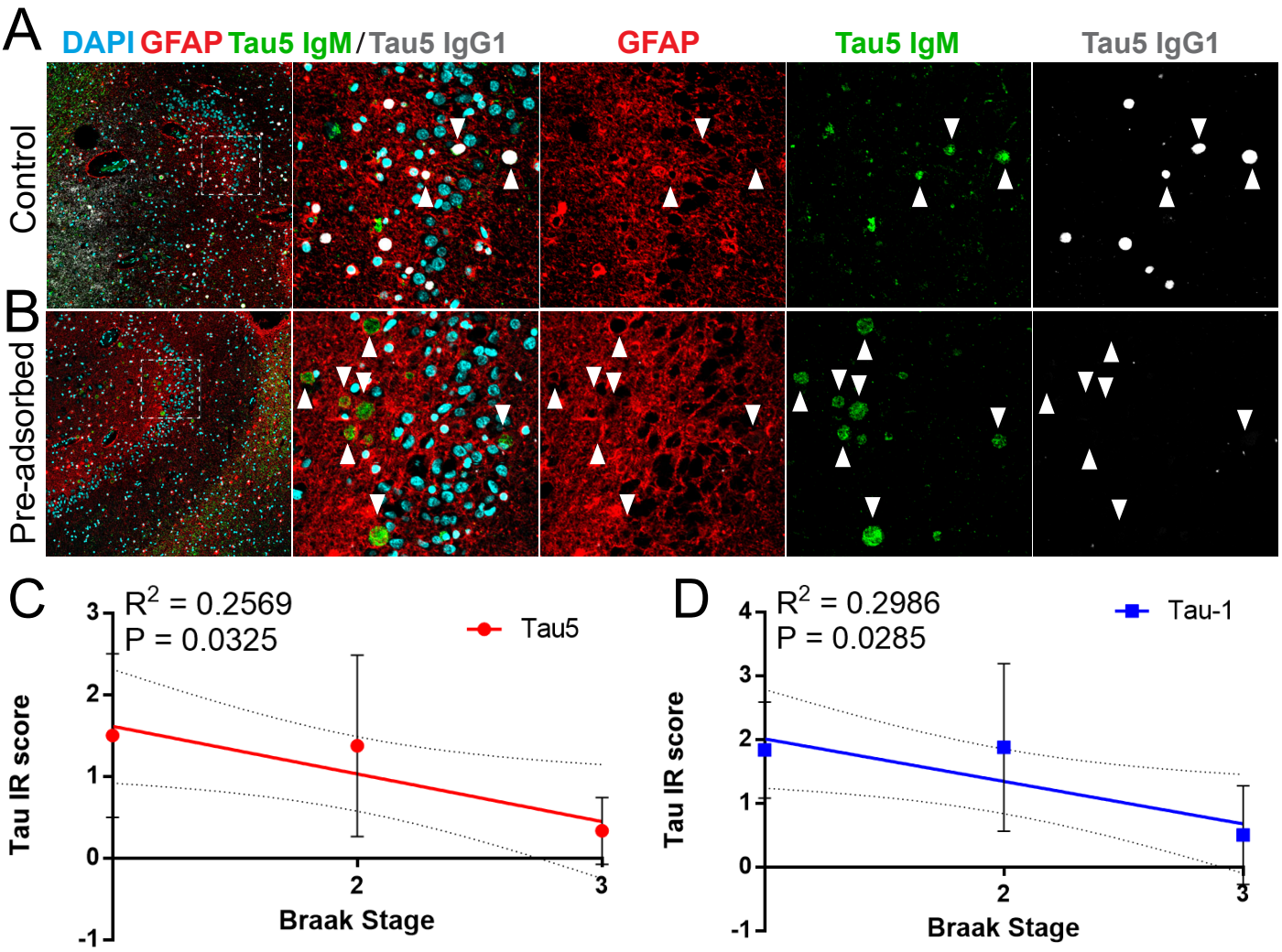

Figure S7. Validation of tau immunoreactivity in human CA by immunoadsorption, Related to Figure 7

(A) Immunofluorescent confocal image of the hippocampus of an aged, healthy human control patient (Control) immunostained with tau5 and GFAP and labeled with anti-mouse IgM μ-chain specific (Tau5 IgM, green), anti-mouse IgG1-specific (Tau5 IgG1, grey), and anti-rabbit IgG (GFAP, red) secondary antibodies. CA are immunoreactive for both Tau5 IgM and Tau5 IgG1 (B) Immunofluorescent confocal image of the hippocampus of an aged, healthy human control patient immunostained with pre-adsorbed tau5 antibody. Anti-mouse IgG1-specific signal (Tau5 IgG1, grey) is eliminated in pre-adsorbed samples, whereas the anti-mouse IgM μ-chain specific (Tau5 IgM, green) signal remains in CA. (C) Human control and AD patients (demographics and details are listed in Table S3) were analyzed for tau5 immunoreactivity within CA in IHC stained sections from the hippocampal sulcus. Correlation analysis of tau5 immunoreactivity scores were plotted as a function of increasing Braak stage. (D) Similar correlation analysis of tau-1 immunoreactivity was performed as a function of Braak stage.

Table S1. Primary Antibodies Used in this Study, Related to All Figures

Green highlights indicate positive IgM immunoreactivity and red indicates positive IgG specific immunoreactivity within granules

Antibody	Host	IgM IR	Granule IR	Source	Catalog Number
Anti-Tau-1 Antibody, clone PC1C6	Ms	+	+, IgG2a	EMD Millipore	MAB3420
Anti-Tau (T22), oligomeric Antibody	Rb	+	n/a	Millipore	ABN454
MAP2	Rb	+	n/a	Millipore	AB5622
MAP2	Ms	+	-	Millipore	MAB3418
Tau5	Ms	+	+, IgG1	Invitrogen	AHB0042
APP (6E10)	Ms	-	n/a	Covance	SIG-39320
K9JA (Pan-Tau)	Rb	-	n/a	Dako	A0024
AT8	Ms	-	n/a	Thermo Fisher Scientific	MN1040
Reelin (G10)	Ms	+	+, IgG1	Abcam	Ab78540
GFAP	Rb	-	n/a	Dako	Z0334
GFAP (GA5)	Ms	+	+, IgG1	millipore	MAB360
Iba1	Rb	-	n/a	Wako	019-19741
Mouse IgG2a kappa Isotype Control (eBM2a)	Ms	-	-	eBiosciences	14-4724-82

Table S2. Secondary Antibodies Used in this Study, Related to All Figures

Secondary Antibodies	Isotype Specificity	Source	Catalog Number
Goat anti-Mouse IgG1 Cross-Adsorbed Secondary Antibody, Alexa Fluor 647	Ms IgG1	Thermo Fisher	A-21240
Goat anti-Mouse IgG1 Cross-Adsorbed Secondary Antibody, Alexa Fluor 594	Ms IgG1	Thermo Fisher	A-21125
Goat anti-Mouse IgG2a-Cross-Adsorbed Secondary Antibody, Alexa Fluor 594	Ms IgG2a	Thermo Fisher	A-21135
Goat anti-Mouse IgM (Heavy chain) Cross-Adsorbed Secondary Antibody, Alexa Fluor 488	Ms IgM	Thermo Fisher	A-21042
Goat Anti-Mouse IgM, µ chain specific Alexa Fluor 488 AffiniPure	Ms IgM	Jackson Immuno	115-545-075
Goat anti-Rabbit IgG (H+L) Cross-Adsorbed Secondary Antibody, Alexa Fluor 568	Rb IgG	Thermo Fisher	A-11011
Goat Anti-Rabbit IgM mu chain Alexa Fluor 488	Rb IgM	Abcam	ab150093
Goat anti-Rabbit IgG (H+L) Cross-Adsorbed Secondary Antibody, Alexa Fluor 594	Rb IgG	Thermo Fisher	A-11012
Donkey anti-Mouse IgG (H+L) Highly Cross-Adsorbed Secondary Antibody, Alexa Fluor 488	Ms IgG	Thermo Fisher	A-21202
Donkey anti-Mouse IgG (H+L) Highly Cross-Adsorbed Secondary Antibody, Alexa Fluor 568	Ms IgG	Thermo Fisher	A-10037
Donkey anti-Mouse IgG (H+L) Highly Cross-Adsorbed Secondary Antibody, Alexa Fluor 647	Ms IgG	Thermo Fisher	A-31571
Donkey anti-Rabbit IgG (H+L) Highly Cross-Adsorbed Secondary Antibody, Alexa Fluor 488	Rb IgG	Thermo Fisher	A-21206
Donkey anti-Rabbit IgG (H+L) Highly Cross-Adsorbed Secondary Antibody, Alexa Fluor 568	Rb IgG	Thermo Fisher	A-10042
Donkey anti-Rabbit IgG (H+L) Highly Cross-Adsorbed Secondary Antibody, Alexa Fluor 647	Rb IgG	Thermo Fisher	A-31573
Goat anti-Mouse IgG1 Cross-Adsorbed Secondary Antibody, HRP	Ms IgG1	Thermo Fisher	A10551
Goat anti-Mouse IgG2a Secondary Antibody, HRP	Ms IgG2a	Thermo Fisher	A-10685

Table S3. Human Patient Demographics, Related to Figure 7 Patients are organized by neuropathological diagnosis including demographic and pathological data. Semi-quantitative analysis of the tau-immunoreactive intensity of CA (for AT8, tau-1, and tau5) in the hippocampal sulcus for each sample was performed using an ordinal rating scale (0=none, 0.5= rare faint CA tau reactivity, 1=mild, infrequent CA tau reactivity, 2= moderate consistent CA tau reactivity and 3= severe consistent CA tau reactivity) similar to previously described methods (Montine et al., 2012). While we did not observe AT8 reactivity within CA, we note occasional AT8 reactive dystrophic neurites surrounding CA. N/A denotes instances where tissues were excluded from semi-quantitative analysis, or where Braak staging was not available.

Age	Sex	Clinical Diagnosis	Fixation Type	CA	AT8	tau5	tau-1	Braak03	Braak06	CERAD	AD
64	Female	Normal	Formalin	++	0	3	3	1	1	0	LOW
70	Female	Normal	Formalin	+	0	2	2	1	1	0	LOW
70	Male	Normal	Formalin	+	0	0.5	1	1	1	1	LOW
75	Female	Normal	Formalin	+++	0	2	2	1	1	0	LOW
74	Female	Probable Alzheimer's Disease	Formalin	+	0	1	3	2	3	3	MED
87	Male	Mild cognitive impairment (Amnestic)	Formalin	+++	0	0.5	0.5	2	4	0	MED
64	Male	Probable Alzheimer's Disease	Formalin	n/a	0	0	0	3	6	3	HIGH
83	Male	Probable Alzheimer's Disease	Formalin	++	0	0	0	3	6	3	HIGH
86	Male	Probable Alzheimer's Disease	Formalin	n/a	0	0	0	3	6	3	HIGH
94	Female	Normal	Formalin	+++	0	0.5	0.5	3	5	1	HIGH
56	Female	Normal	Ethanol	++	0	1	2	1	n/a	0	NO
83	Male	Schizophrenia	Ethanol	n/a	0	0.5	1	1	n/a	0	NO
84	Male	Parkinson's Disease (not demented)	Ethanol	n/a	0	1	1	2	n/a	2	MED
65	Female	FTLD-NOS	Ethanol	+++	0	0.5	0.5	3	5	1	HIGH
72	Female	Corticobasal syndrome	Ethanol	+++	0	3	3	2	6	3	HIGH
76	Female	Probable Alzheimer's Disease	Ethanol	n/a	0	1	2	3	n/a	3	HIGH
84	Male	Probable Alzheimer's Disease	Ethanol	++	0	0	0.5	3	6	3	HIGH

Transparent Methods

Animals

All protocols were carried out in accordance with the University of North Carolina (UNC) Institutional Animal Care and Use Committee (UNC IACUC protocol 19.017). Mice were anesthetized with isoflurane and perfused with 1X PBS and 15mL 4% Paraformaldehyde. Brains were then fixed for 24 hr in 4% PFA at 4°C and then cryoprotected in a 30% sucrose gradient before sectioning. Tau knockout (TKO) mice are commercially available (Jackson Laboratory, #7251) and were used to confirm the loss of tau-immunoreactive granules by immunofluorescence. 3xTg-AD (AD) mice are commercially available (Jackson Laboratory, #34830) and were used to detect accelerated granule formation in a tau transgenic AD model. Male and female mice were used in equal numbers, as there were no apparent differences in the biochemistry or histology phenotypes examined in this study. All mouse ages and time-points examined were carefully documented and reported in the figure legends. Mice were housed in groups of 3-5 during aging. All transgenic animals were genotyped using PCR and primers for the respective transgenes. Animals that sustained visible injuries due to aggression or displayed aberrant health conditions were excluded from the study.

Immunoadsorption

Map-rich tubulin (Cytoskeleton, Inc) was purified using a standard tubulin protocol (temperature-induced tubulin polymerization and ionic exchange chromatography). For adsorption and western blot experiments, the lyophilized powder was resuspended in 100mM sodium acetate, pH 7.0. Sodium acetate was also used as the resuspension buffer in recombinant full-length wild type (2N4R tau) and tau-1 peptide (^{189}pksgdrsgysspgspgtpg^{207}) suspensions. Primary antibodies were incubated for 24 hr at 4°C on a rotating wheel in blocking buffer (1% goat serum in 1X TBS + 0.01% thimerosal) mixed with sodium acetate at equal concentrations between adsorption and control conditions before application to tissues for the primary antibody stain.

Immunoblotting and biochemical analyses

Cell lysates and mouse brain fractions were resolved via SDS-PAGE on 10% gels, transferred to nitrocellulose membrane (Biorad), and blocked with 2% milk in 1X TBS for 30 min. Membranes were rinsed in 1X TBST (Tris- Buffered Saline + 0.1% Tween) for 3 x 5 min between each blotting step. Membranes were incubated with primary antibody in blocking solution overnight at 4 °C, followed by a 1 hr room temperature incubation with HRP-conjugated anti-mouse or anti-rabbit antibodies (1:1000). The following primary antibodies were used in this study for immunoblotting: AT8 (Thermo, MN1020, 1:500), K9JA (DAKO, A0024 1:1000), TauY9 (Enzo BML-TA3119-0100, 1:1000).

Immunofluorescence (IF) - mouse tissue

Mice were deeply anesthetized and transcardially perfused with 1X PBS and 15 mL 4% Paraformaldehyde. Brains were then post-fixed for 24 hr in 4% PFA at 4°C and cryoprotected in 30% sucrose solution before sectioning. Tissues were sectioned at 40 μm thickness and stored at -20°C. Immunofluorescence staining was conducted using a free-floating technique, rinsing in 1X TBS between all major steps, gently agitated on a plate shaker. Sections were rinsed and permeabilized for 50 minutes in 2% TBS-Triton X-100 at RT. Blocking, primary, and secondary

solutions matched the donor species of secondary antibodies used; sections were blocked in 1X TBS with 1% donkey serum for non-isotype specific stains and blocked in 1% goat serum for isotype specific stains for 50 min each. Sections were then incubated with primary antibody in 0.1% sodium azide solution for 48 hr at room temperature, thoroughly rinsed, and incubated in secondary antibody solution for 24 hr at room temperature. Note that adsorption experiments were performed with 0.01% thimerosal in 1X TBS to exclude the possibility of sodium azide-mediated antibody binding interference. Immunofluorescence staining was performed using the primary and secondary antibodies detailed in Tables S1 and S2. Primary antibody dilutions: tau5 1:200, tau-1 1:1000, AT8 1:200, T22 1:1000, Reelin 1:1000, GFAP 1:1000, Iba1 1:1000. Secondary antibody dilutions: Alexa Fluor goat anti-mouse IgM μ-chain specific 488 1:200, Alexa Fluor goat anti-rabbit 568 1:500, Alexa Fluor goat anti-mouse IgG1 specific 647 1:200, Alexa Fluor goat anti-mouse IgG2a specific 594 1:200, Alexa Fluor goat anti-mouse IgG2a specific 647 1:200.

Immunofluorescence (IF) - human tissue

Human brain sections used for immunofluorescence were provided by the UNC Translational Pathology Lab (TPL), which maintains a catalogued AD brain repository with neuropathologically confirmed AD cases. Human hippocampal brain sections were formalin fixed, paraffin embedded, and sectioned at 7 μm. Sections were deparaffinized in xylene two times for 45 min each and then rehydrated using a 100%-70% EtOH gradient, 5 min water rinse, followed by overnight hydration in 1X PBS. Antigen retrieval was conducted with Vector Labs Citric Acid Based Antigen Unmasking Solution, pH 6.0, (H-3300). Sections were incubated in 0.5L of 1X solution; held at rolling boil for 10 min, incubated for 10 min on hot plate, and then another 10 min at room temperature before being rinsed in 1X PBS for 5 min. Sections were then immunostained using the previously described immunofluorescent reagents, antibodies, and methods, and mounted in Fluoromount G for confocal imaging. Primary antibody dilutions: tau5 1:200, GFAP 1:1000. Secondary antibody dilutions: Alexa Fluor goat anti-mouse IgM μ-chain specific 488 1:200, Alexa Fluor goat anti-rabbit 568 1:500, Alexa Fluor goat anti-mouse IgG1 specific 647 1:200.

Immunofluorescence (IF) analysis

Image preparation and analysis was conducted in ImageJ on pseudocolored images obtained on the Olympus FV3000RS confocal microscope. For tau-1_{IR} granule quantification, brain sections were imaged at 40x magnification with identical exposure settings and analyzed at normalized brightness and contrast levels (ImageJ). Tau granules were manually counted from N = 4 hippocampal sections per animal by an investigator blinded to genotype, and densities (granules/mm^3) were measured by dividing the total number of granules per ROI volume. Granules were counted when meeting all of the following criteria: spherical immunofluorescence signal above background, ranging in size from 1-5 μm, and present in groups of 5 or more granules within a ~ 40 μm diameter. All quantitative fluorescence was independently validated with a minimum of N = 3 biological replicates per genotype. 3D reconstruction analysis of PAS granule was performed using IMARIS Bitplane software. Images were surfaced with (Fig. 6A-B) and without (Fig. 6C) smoothing and processed with preset background subtraction.

Microscopy
Confocal images were captured on an Olympus FV3000RS microscope using resonant, one-way scanning at 512x512 resolution. The following fluorophores were used: Alexa Fluor 405 (DAPI), Alexa Fluor 488, Alexa Fluor 568, Alexa Fluor 594, Alexa Fluor 647. Laser intensities, gains, and offsets were set at thresholds that reflect minimal fluorescence in respective control stains of sections incubated with only blocking buffer and secondary antibodies for each experiment. Imaging parameters were tailored each experimental application, but were kept consistent between genotypes, adsorption pairs, and all other respective experimental and control stains; sections used for quantification of tau-1_{IR} granules were imaged at 20x magnification with 2x zoom. For co-localization and immunoadsorption analysis, sections were imaged at 20x magnification with 3x zoom, and fluorescence channels (488, 568, 594/647) were sufficiently separated to minimize the possibility of cross-channel fluorescence. Phase separation ensured that fluorescence spectra did not significantly overlap (pairing: 405+568/594, 488+647, when applicable). High-resolution images for glial association comparisons and 3D reconstruction images were captured using 60x magnification and 2x zoom.

Immunohistochemistry (IHC)
For human IHC studies, fixed, paraffin-embedded tissue blocks from the hippocampal gyrus were performed in conjunction with the Center for Neurodegenerative Disease Research (CNDR) Brain Bank at the University of Pennsylvania. The demographics of all cases are listed in Table S3. Consent for autopsy was obtained from legal representatives for all subjects in accordance with local institutional review board requirements. At the time of autopsy, tissues from each brain were fixed with either 70% ethanol or neutral buffered formalin in 150 mM NaCl, infiltrated with paraffin, and cut into 6-µm serial sections. IHC was performed using the avidin-biotin complex (ABC) detection system (Vector Laboratories, Burlingame, CA) and 3,3'-diaminobenzidine. Briefly, sections were deparaffinized and rehydrated, endogenous peroxidases were quenched with 5% H2O2 in methanol for 30 min, and sections were blocked in 0.1 mol/L Tris with 2% fetal bovine serum for 5 min. Primary antibodies were incubated overnight at 4°C. After washing, sections were sequentially incubated with cross-adsorbed anti-mouse anti-IgG1 or anti-IgG2a secondary antibodies conjugated to HRP for tau5 and tau-1 primary antibodies, respectively (Table 2) for 1 hr and ABC for 1 hr. AT8 used species-specific secondary antibody. Bound antibody complexes were visualized by incubating sections in a DAB solution (Vector Laboratories, Burlingame CA) for 6 min. Sections were then lightly counterstained with hematoxylin, dehydrated, and mounted on coverslips. Sections were imaged using a whole-slide scanner (Aperio AT2 Scan Scope, Leica, Wetzlar, Germany). Primary antibody dilutions were used at the following: tau5, 1:200; tau-1, 1:1000; AT8, 1:200.

Dual in situ hybridization and immunofluorescence (ISH/IF)
Mouse tissues were collected via 4% PFA fixation as previously described and sectioned on a cryostat at 16 µm thickness, mounted on slides, and stored at -80°C prior to use. RNAscope reagents and probes were used in accordance with the manufacturer recommended protocol for the FAST-RED system (Wang et al., 2012), but slightly adapted for dual ISH and IF. Briefly, slides were air-dried for 30 min at 60°C, rinsed in 1X PBS for 5 min, then post-fixed in 4% PFA in 1X PBS for 14 min at 4°C. Slides were then dehydrated in successive incubations in 50%, 70% and 100% ETOH for 5 min each, air dried, and then incubated in RNAscope hydrogen peroxide for 10 min at RT. Slides were immersed in hot (98-102°C) antigen retrieval buffer for

5 min, immediately rinsed in distilled water 2 x 1 min, and then 100% EtOH before drying. Slides were then exposed to RNAscope protease for 30 min at 40°C in the ACDBio HybEZ oven. All probe and amplification steps were conducted in the humidity controlled HybEZ oven, and rinsed twice with RNAscope 1X wash buffer after each step: Tissue sections were covered by RNAscope probe solutions and incubated for 2 hr at 40°C. Subsequent amplification reagents were applied in sequence within the HybEZ oven and tray according to specifications. After hybridization protocols, tissues were rinsed in 0.1M PBST and then permeabilized in 0.1M PBST 0.5% Triton X-100. Tissues were blocked and antibody solutions prepared in 0.1M PBST 2% donkey serum followed by 48 hr primary antibody incubation at RT and 24 hr secondary antibody incubation at RT. Immunofluorescence (IF) staining was conducted with Alexa Fluor donkey anti-rabbit and anti-mouse secondaries described previously. Several antibodies were used for IF at optimized concentrations: GFAP (Abcam, 1:250), T22 (Millipore, 1:250).

Experimental Design and Statistical Analyses

GraphPad Prism software was used for all statistical analyses. Results were polled from a minimum of N = 3 biological replicates and presented as average ± standard deviation of the mean (SD). Statistical analysis was determined using a two-tailed unpaired Student's t-test with equal variance (significance set as $p < 0.05$). R^2 and p-values for tau immunoreactivity correlation with Braak stage was conducted using 16 datapoints from postmortem brain tissue analysis using blinded semi-quantitative methods. The number and demographics of human postmortem cases analyzed by IHC are described in Table S3.

Supplemental References

Montine, T. J., Phelps, C. H., Beach, T. G., Bigio, E. H., Cairns, N. J., Dickson, D. W., Duyckaerts, C., Frosch, M. P., Masliah, E., Mirra, S. S., Nelson, P. T., Schneider, J. A., Thal, D. R., Trojanowski, J. Q., Vinters, H. V., Hyman, B. T., National Institute On, A. & Alzheimer's, A. 2012. National Institute on Aging-Alzheimer's Association guidelines for the neuropathologic assessment of Alzheimer's disease: a practical approach. *Acta Neuropathol,* 123**,** 1-11.

Wang, F., Flanagan, J., Su, N., Wang, L. C., Bui, S., Nielson, A., Wu, X., Vo, H. T., Ma, X. J. & Luo, Y. 2012. RNAscope: a novel in situ RNA analysis platform for formalin-fixed, paraffin-embedded tissues. *J Mol Diagn,* 14**,** 22-9.